The Ribosome Maturation Factor Rea1 utilizes nucleotide independent and ATP hydrolysis driven Linker remodelling for the removal of ribosome assembly factors

Johan Busselez[1,2,3,4], Geraldine Koenig[1,2,3,4], Torben Klos[1,2,3,4], Hugo Gizardin-Fredon[5], Sarah Cianferani[5], Carine Dominique[6], Yves Henry[6], Anthony Henras[6] & Helgo Schmidt[1,2,3,4,*]

1. *Institut de Génétique et de Biologie Moléculaire et Cellulaire, Integrated Structural Biology Department, Illkirch, France*
2. *Centre National de la Recherche Scientifique, UMR7104, Illkirch, France*
3. *Institut National de la Santé et de la Recherche Médicale, U1258, Illkirch, France*
4. *Université de Strasbourg, Illkirch, France*
5. *Laboratoire de Spectrométrie de Masse BioOrganique, Université de Strasbourg, CNRS UMR7178, IPHC, Strasbourg, France*
6. *Molecular, Cellular and Developmental Biology Unit (MCD), Centre de Biologie Intégrative (CBI), Université de Toulouse, Toulouse, France*

*Corresponding author

Summary

The essential ribosome maturation factor Rea1 (also known as Midasin) catalyses the removal of assembly factors from precursors of the large ribosomal subunit and subsequently promotes their export from the nucleus to the cytosol. Rea1 is a large protein of nearly 5000 residues and a member of the AAA+ (ATPases associated with various cellular activities) protein family. It consists of a concatenated ring of six AAA+ domains from which the ≈ 1700 residue linker emerges that is subdivided into stem, middle and top domains. A flexible and unstructured D/E rich region connects the linker top to a MIDAS (metal ion dependent adhesion site) domain, which is able to bind the assembly factor substrates. Despite its key importance for ribosome maturation, the Rea1 mechanism driving assembly factor removal is still poorly understood. Although early studies on Rea1 demonstrated that assembly factor removal requires ATP hydrolysis, the Rea1 conformations associated with ATP hydrolysis have not been identified yet. Here we demonstrate that the Rea1 linker is essential for assembly factor removal. It rotates and swings towards the AAA+ ring following a complex remodelling scheme involving nucleotide independent as well as nucleotide dependent steps. ATP hydrolysis is required to engage the linker top with the AAA+ ring and ultimately with the AAA+ docked MIDAS domain. The interaction between the linker top and the MIDAS domain allows force transmission for assembly factor removal.

Introduction

Ribosomes are essential for protein synthesis and their production of ribosomes is the most energy consuming process in cells. It is estimated that exponentially growing cells spend XX% of their energy

production on ribosome biosynthesis. In eukaryotes more than 200 assembly factors are involved in the production of ribosomes [1]. Ribosome assembly starts in the nucleolus with the transcription of the 5S and 35S rRNAs by RNA polymerases III and I, respectively. The 35S rRNA is subsequently cleaved into a smaller 20S and a larger 27S part. The 20S rRNA forms the basis of the future 40S ribosomal subunit. The 27S rRNA associates with various ribosomal proteins, ribosomal assembly and maturation factors as well as the 5S rRNA to form pre-60S ribosomal (pre-60Sr) particles [2]. These particles are subsequently exported to the cytosol via the nucleoplasm. During this process, they are gradually transformed into mature 60S subunits by transiently interacting with additional assembly factors that promote conformational rearrangements and rRNA processing steps [2]. The 60S assembly intermediates have been extensively studied using *Saccharomyces cerevisiae* as a model organism [3, 4]. One of the earliest assembly intermediates identified in the nucleolus is a pre-60Sr particle that carries the Ytm1 complex, consisting of Ymt1, Erb1 and Nop7 [5] and involved in the processing of the 27S rRNA [6]. To promote transfer of this particle to the nucleoplasm, the Ytm1 complex has to be removed, a reaction that is carried out by Rea1 (also known as “Ylr106p” or “Midasin”) [7, 8]. Rea1 associates with pre-60Sr particles via its interaction with the Rix1 complex, which consists of Rix1, Ipi1 and Ipi3 [9, 10]. The Rea1 catalysed removal of the Ytm1 complex is absolutely essential for the nucleoplasmic export of pre-60Sr particles, because disrupting the interaction between Rea1 and Ytm1 leads to the accumulation of pre-60Sr particles in the nucleolus [8].

In the nucleoplasm, pre-60Sr particles bind to the assembly factor Rsa4, which tightly associates with another assembly factor, Nsa2. Nsa2 wraps around the H89 rRNA helix of the immature peptidyltransferase center [11-13]. In addition to the Ytm1 complex, Rea1 also mechanically removes Rsa4 from pre-60Sr particles [10]. In doing so, it might indirectly force Nsa2 to pull on the H89 rRNA helix to drag this important architectural feature of the peptidyltransferase center into its correct position [11].

In addition to indirectly stimulating the remodelling of the pre-60Sr particles by removing Rsa4, Rea1 and the Rix1 complex also directly contribute to maturation. One of the most prominent consequences of Rea1/Rix1 complex binding to pre-60Sr particles is a 180° rotation of the 5S RNP complex towards it mature position [14]. This remodelling step strictly requires the binding of both factors, Rea1 and the Rix1 complex [14].

The Rea1 mediated Rsa4 removal is also crucial for the export of pre-60Sr particles from the nucleoplasm to the cytosol. The removal of Rsa4 leads to an activation of the GTPase activity of Nug2 [15], another pre-60Sr particle associated assembly factor. Subsequently, Nug2-GDP dissociates from the pre-60Sr particle which allows the nuclear export factor Nmd3 to bind to the former Nug2 site. Nmd3 in turn associates with Crm1 and RanGTP to trigger the export of pre-60Sr particles to the

cytosol [15]. Disrupting the Rea1-Rsa4 interaction leads to the accumulation of pre-60Sr particles in the nucleoplasm and severe growth defects in *S. cerevisiae* [10], demonstrating the importance of Rea1 also for the nucleoplasmic export of pre-60Sr particles.

Rea1 is conserved from yeast to mammals and related to the motor protein dynein [16]. Its deletion in yeast leads to non-viable strains [16, 17] underscoring the essential role of this complex molecular machine, which consists of nearly 5000 amino-acid residues. Rea1 folds into a concatenated hexameric ring of six AAA+ (ATPases associated with various cellular activities) domains, each divided into large (AAAL) and small sub domains (AAAS). From the hexameric AAA+ ring a ≈ 1700 amino-acid linker domain emerges, consisting of stem-, middle- and top subdomains [18] (Figure 1A). The linker top2 domain connects to a ≈ 600 amino-acid glutamate and aspartate rich region which ends in a ≈ 300 amino-acid metal ion dependent adhesion site (MIDAS) domain [16, 18-20] (Figure 1A). The MIDAS domain interacts with the ubiquitin like (UBL) domains of Ytm1 and Rsa4 [8, 10]. The interaction is mediated by a Mg^{2+} ion and resembles the integrin MIDAS – ligand interaction [10, 21]. The MIDAS domain is able to dock onto the AAA+ ring [18, 20] and in the context of the Rea1-pre60S particle complex this docking site places the MIDAS domain in direct contact with the Rsa4 UBL domain [19]. Recently, the catch bond character of the interaction between the Rea1 MIDAS and the Ytm1 and Rsa4 UBL domains has been demonstrated with forces up to 4 pN increasing the lifetime of the interaction [22].

The question how force is transmitted to the substrate engaged MIDAS domain to remove Rsa4 or Ytm1 from pre60S particles has been controversial. Ytm1 and Rsa4 *in-vitro* releases assays have established that the force production for assembly factor removal from pre60S particles requires ATP-hydrolysis [8, 10], but so far no Rea1 conformations associated with ATP-hydrolysis have been described. Early hypotheses suggested the Rea1 tail with the MIDAS domain at its top would move essentially as a rigid body and switch during ATP hydrolysis in the Rea1 AAA+ ring from pre60S proximal conformations to engage with assembly factors and pre60S distal conformations to remove them from pre60S particles [10]. However, recent high-resolution cryoEM studies did not detect nucleotide dependent Rea1 linker remodelling [18, 20]. It even has been suggested that the linker remodelling might not be relevant for assembly factor removal suggesting instead that nucleotide driven conformational rearrangements in the AAA+ ring are directly communicated to the AAA+ ring docked, substrate engaged MIDAS domain to produce the force for assembly factor removal [20, 23].

Here we provide evidence for the functional importance of the Rea1 linker region and demonstrate nucleotide independent as well as ATP hydrolysis dependent linker remodelling in Rea1. We show that linker remodelling consists of two main components, a rotation of the linker middle and top domains relative to the linker stem domain and a pivot movement towards the AAA+ ring.

Furthermore, we demonstrate that linker remodelling is able to produce mechanical force. In the final remodelling step, the linker top interacts with the AAA+ ring docked MIDAS domain allowing direct transmission of force for assembly factor removal. Our results reveal key mechanistic events of one of the most complex eukaryotic ribosome maturation factors whose mode of action has remained elusive since the first description of Rea1 20 years ago.

Results

The Rea1 linker middle and top domains are functionally important

In order to investigate the functional relevance of the Rea1 linker region, we created a Rea1 construct with deleted linker top and middle domains and fused the MIDAS domain and D/E rich region directly to the linker stem (Rea1$\Delta_{middle\text{-}top}$) (Fig. 1B). Next we tested the functionality of Rea1$\Delta_{middle\text{-}top}$ using a modified version of a *Saccharomyces cerevisiae* GFP-Rpl25 pre60S export assay [10]. In this assay, the ability of a Rea1 construct to promote the nuclear export of pre60S particles is monitored by the occurrence of GFP fluorescence in the cytoplasm. We tagged the endogenous Rea1 gene with the auxin degron system, provided a plasmid encoding Rea1$\Delta_{middle\text{-}top}$ and monitored the cellular GFP fluorescence distribution after auxin induced degradation of endogenous Rea1 (Fig. 1C). Consistent with a crucial functional role of the linker top and middle domains in pre60S particle nuclear export, we observe the accumulation of GFP-fluorescence in the nucleus (Fig. 1D).

The Rea1 linker undergoes nucleotide independent as well as nucleotide dependent remodelling

Having established the functional importance of the linker region, we decided to investigate the nucleotide depended conformational changes of the Rea1 linker. Recently, we [18] and other groups [20] aimed at the determination of 3D structures of distinct linker conformations by electron microscopy (EM), but were not able to visualize linker remodelling. We reasoned that such an approach might fail to detect alternative linker conformations if they are in low abundance and/or classify into a limited number of 2D views thereby precluding the calculation of interpretable 3D EM maps.

We decided to analyse Rea1 nucleotide dependent linker remodelling by negative stain EM. Compared to cryo-electron microscopy, negative stain EM offers the advantage of increased signal-to-noise ratios for individual particles, which should ease the detection of low abundance Rea1 linker conformations. We reasoned that even though the resolution of negative stain EM is limited, large scale remodelling events of the ≈200 kDa linker domain should still be detectable. We also limited our image processing workflow at the 2D classification stage and did not attempt to calculate 3D EM maps

to avoid failing to detect alternative linker conformation due to insufficient 2D projection distributions.

First, we characterized wild-typ *S. cerevisiae* Rea1 in the presence of ATP. We were able to obtain several 2D classes with identical top view onto the AAA+ ring. In these 2D classes the linker samples a range of different conformations with respect to the AAA+ ring as illustrated in Fig. 1E. We tentatively sorted them into "Extended", "Intermediate" and "AAA+ ring engaged" linker conformations" and assigned the numbers 1 - 7 from the most extended to the most compact Rea1 linker state (Fig. 1E). States 6 and 7, which represent the AAA+ ring engaged linker conformations are clearly minority classes representing only ≈ 0.8% of the total particles in the data set. States 1 – 3 of the extended and state 4 of the intermediate linker conformations are similar to Rea1 linker conformations described in earlier studies [10] (Supplementary figure 1). In the nucleotide free, APO data set AAA+ ring top view particles exclusively sorted into the extended and intermediate linker conformations (states 1 - 5) (Fig. 1E), suggesting that the AAA+ ring engaged linker conformations require the presence of nucleotide. To further investigate whether ATP binding or hydrolysis is needed to engage the linker with the AAA+ ring, we collected a negative stain data set in the presence of the non-hydrolysable ATP analogue AMPPNP. Again, only the extended and intermediate linker conformations were sampled (states 1 - 5) (Fig. 1E) indicating that linker AAA+ ring engagement requires ATP-hydrolysis.

Collectively, these results demonstrate that distinct Rea1 linker remodelling steps exist. The extended and intermediate linker conformations are being sampled even in the absence of any nucleotide highlighting the intrinsic conformational flexibility of the linker. The AAA+ ring engagement of the linker requires ATP hydrolysis, which suggests an important functional role for these low abundance conformations. This view is also supported by Rsa4 and Ymt1 *in-vitro* release assays that demonstrated that only ATP but not AMPPNP enables Rea1 to catalyse the removal of its assembly factor substrates from pre60S particles [8, 10]. These findings indicate that the extended and intermediate linker conformations (states 1 – 5) (Fig. 1E) are insufficient to support functionality and that additional conformations linked to ATP hydrolysis (states 6 and 7) have to be sampled to catalyse assembly factor removal.

Next, we investigated a Rea1 mutant ($Rea1_{\Delta AAA2H2\alpha}$) lacking the AAA2 helix 2 α-helical insert (AAA2H2α). In a previous study we demonstrated that AAA2H2α is an auto-inhibitory regulator of the Rea1 ATPase activity that also prevents the docking of the MIDAS domain onto the AAA+ ring [18]. The relocation of AAA2H2α from the central pore of the AAA+ ring and the docking of the MIDAS domain onto the AAA+ ring is also observed when Rea1 is bound to Rsa4-pre60S particles [14, 19]. This suggests that the $Rea1_{\Delta AAA2H2\alpha}$ mutant resembles Rea1 when bound to pre60S particles. We wanted to investigate if and how linker remodelling is altered in $Rea1_{\Delta AAA2H2\alpha}$.

We determined negative stain EM 2D class averages of the ATP, ADP and AMPPNP states. In the presence of ATP, the AAA+ ring top view particles sorted again in extended, intermediate as well as AAA+ ring engaged classes (Fig. 2). The linker conformations are highly similar to the ones observed for the Rea1 wt (Fig. 1E) suggesting that linker remodelling is not altered in the $Rea1_{\Delta AAA2H2\alpha}$ mutant. Incubating $Rea1_{\Delta AAA2H2\alpha}$ with ADP or AMPPNP restricts linker remodelling to the extended and intermediate classes (Fig. 2) indicating that - like in the case of Rea1 wt - ATP-hydrolysis is required for linker AAA+ ring engagement. AAA+ ring engaged classes are again minority views representing only ≈0.4% of the total particles in the ATP data set.

Recent cryoEM studies on a AAA+ unfoldase made use of the slowly hydrolysable ATP analogue ATPγS to enrich transient protein conformations [24]. To evaluate if ATPγS might also enrich the AAA+ ring engaged linker conformations, we incubated $Rea1_{\Delta AAA2H2\alpha}$ with ATPγS followed by negative stain EM analysis. Although we did not observe a substantial enrichment (≈0.4% ATP vs. ≈1.5% ATPγS), we detected state 8, an additional AAA+ ring engaged linker conformation (Fig. 2). We wanted to investigate, if state 8 also exists in Rea1 wt. To this end we incubated Rea1 wt with ATPγS and characterized the sample by negative stain EM. We detected 2D class averages similar to state 8 of $Rea1_{\Delta AAA2H2\alpha}$, but with less well-defined structural features of the linker indicating increased structural flexibility (Supplementary figure 2). Taken together these observations suggest that the activated $Rea1_{\Delta AAA2H2\alpha}$ mutant closely resembles linker remodelling in wt Rea1, but is able to stably sample state 8 of the AAA+ ring engaged linker conformations.

The Linker middle and top domains rotate and pivot towards the AAA+ ring docked MIDAS domain during remodelling

Since $Rea1_{\Delta AAA2H2\alpha}$ in the ATPγS state revealed the highest number of linker remodelling conformations, we thought to annotate the Rea1 subdomains in the corresponding 2D class averages to analyse Rea1 linker remodelling in more detail. To this end, we determined a 3D cryoEM structure of $Rea1_{\Delta AAA2H2\alpha}$ in the presence of ATPγS (Fig. 3A, B and supplementary figure 3) to generate 2D projections for the subdomain assignment in our negative stain EM 2D classes. We combined data collected on non-tilt and tilt grids to increase the number of particle orientations in our data set. However, consistent with previous cryoEM investigations [18], we could only obtain an interpretable 3D reconstruction showing the linker in the straight, extended conformation already described in previous work (supplementary figure 4) [18-20]. We attribute the lack of additional 3D reconstructions to the low abundance and/or preferred orientation of the alternative linker states.

We generated a 2D projection from the $Rea1_{\Delta AAA2H2\alpha}$ ATPγS cryoEM structure with high similarities to the AAA+ ring in our 2D class averages (Fig. 3C), but the linker part did not resemble any

of the observed linker conformations of the eight states (Fig. 2). By using a different orientation of the Rea1$_{\Delta AAA2H2\alpha}$ ATPγS cryoEM structure, we were able to obtain a 2D projection matching the linker of state 1 but not the AAA+ ring (Fig. 3C). The combination of both projections allowed us to assign the NTD, the six AAA+ domains of the AAA+ ring as well as the linker stem, middle and top domains and the MIDAS domain in state 1 (Fig. 3C). Our analysis also demonstrates that the linker in state 1 has already undergone a rigid-body movement with respect to the AAA+ ring compared to the straight linker conformation in our cryoEM structure. We approximate that the linker has rotated ≈ 30˚ counter clock wise around the long linker axis and bent ≈ 45˚ towards the plane of the AAA+ ring (Supplementary figure 5).

A prominent feature ΔAAA2H2α AAA+ ring in states 1 – 8 is a bright spot on the AAA+ ring, which we interpret as AAA+ ring docked MIDAS domain (Fig. 3C). This feature is absent in the Rea1 wt classes (Fig. 3D and supplementary figure 6), which is consistent with earlier findings demonstrating that the presence of the AAA2 H2 α-helical insert in Rea1 wt interferes with the AAA+ ring docking of the MIDAS domain [18]. We also directly confirmed our MIDAS domain assignment by analysing the Rea1$_{\Delta AAA2H2\alpha\text{-}\Delta MIDAS}$ double mutant (Fig. 3D).

Next, we aligned the eight states onto their AAA+ rings (Fig. 4A, Movie S1). These AAA+ ring alignments suggest that the linker top and middle domains pivot towards the AAA+ ring docked MIDAS domain during linker remodelling. The pivot point during this movement is located between the linker stem and middle domains. These alignments further suggest that the linker middle and top domains rotate during the pivot movement. To better visualize this additional transformation, we aligned states 1 - 8 on the long linker axis (Fig. 4B, Movie S2) to demonstrate the rotation, which occurs during states 1 - 5. The linker top and middle domains approximately behave as a rigid body during the rotation as suggested by a series of 2D projections of the linker top and middle domains rotated around the long linker axis (Supplementary figure 7). We estimate the rotation angle between states 1 and 5 to be ≈ 97˚(Supplementary figure 7). We do not exclude the possibility of additional internal rearrangements of the top and middle domains during the rotation. In the final linker remodelling conformation observed in our data, state 8, the linker top2 and top3 domains are in close proximity to the AAA+ ring docked MIDAS domain (Fig.4A, B, Movies S1, S2).

Collectively these results reveal that the linker top and middle domains undergo a complex series of movements with respect to the linker stem domain and the AAA+ ring during linker remodelling. Compared to the straight linker conformation in Fig. 3A, they rotate and pivot towards the plane of the AAA+ ring in an initial movement to reach state 1. From the position in state 1 they pivot towards the AAA+ ring docked MIDAS domain and further rotate around the long linker axis. The rotation largely happens during states 1-5, that cover the extended and intermediate linker conformations.

Since these states are also observed under APO conditions (Fig. 1E), we conclude that also the rotational movement does not require energy suggesting it is part of the intrinsic conformational flexibility of the Rea1 linker like the corresponding pivot movement. The energy of ATP-hydrolysis is needed to engage the fully rotated linker top and middle domains with the AAA+ ring during states 6 - 8 of the AAA+ ring engaged linker conformations. The connection between the linker and the AAA+ ring in state 6 that separates the AAA+ ring engaged conformations from the intermediate conformations occurs between the linker top3 domain and AAA1S (Supplementary figure 8). In state 8, the linker top2 and top3 domains are in close proximity to the AAA+ ring docked MIDAS domain (Fig. 4A, B). The fact that state 8 was not observed in Rea1 wt, which does not show the AAA+ ring docked MIDAS domain (Fig. 3D and supplementary figure 6), suggests that the presence of the MIDAS domain at the AAA+ ring is essential for sampling state 8.

The Linker top interacts with the MIDAS domain and linker remodelling is a force producing event

Since the linker top 2 and top 3 domains in state 8 are located next to the MIDAS domain, we wanted to test if there is a direct interaction. To this end, we carried out crosslinking mass spectrometry on the $Rea1_{\Delta AAA2H2\alpha}$ mutant in the presence of ATPγS. Although our negative stain EM analysis suggests that state 8 only represents ≈0.2% of the total particles in our sample, we were able to detect a crosslink between K3955 in the top2 domain and K4668 located in a highly conserved loop region of MIDAS domain. We also find a crosslink between K3564, located in the extended top1-top2 linker region that associates with the top2 domain [18], and K1043 in AAA2S (Fig. 5A). The K3955-K4668 and K3564-K1043 crosslinks are consistent with our domain assignments in state 8 (Figure 4A, B) and hint at a direct interaction between the linker top2 and the MIDAS domains.

The top2 domain crosslink partner K4668 is located in the highly conserved E4656-K4700 loop of the MIDAS domain. While the Rea1 MIDAS domain in general resembles the MIDAS domain architecture of integrins [21], it also features Rea1 specific structural elements and the E4656-K4700 loop is one of them. This loop region harbours an NLS sequence that is required for the nuclear import of Rea1 [21]. It was also demonstrated that the E4656-K4700 loop is essential for assembly factor removal. Deleting and replacing it with an alternative NLS sequences prevented Rea1 from removing its Rsa4 assembly factor substrate from pre60S particles [21].

In order to probe if linker remodelling is able to produce mechanical force, we employed total-internal-reflection-fluorescence (TIRF) microscopy based microtubule gliding assays typically used to probe the motor activity of kinesin or dynein constructs. We worked with the $Rea1_{\Delta AAA2H2\alpha}$ background since this construct shows elevated ATPase activity compared to the wt [18]. We anticipated that the flexible, unstructured and highly negatively charged D/E rich region (theoretical pI: 3.77) of Rea1 might

interfere with the microtubule gliding assay and aimed for the expression of Rea1$_{\Delta AAA2H2\alpha+\Delta D/E\text{-}MIDAS}$, a construct truncated at the end of the top2 domain. However, we could not obtain expression. We screened a truncation series and identified Rea1$_{\Delta AAA2H2\alpha+\Delta 4168\text{-}4907}$, which lacks ≈ 80% of the D/E rich region and the MIDAS domain, as the minimal construct for which we could obtain expression. We further modified Rea1$_{\Delta AAA2H2\alpha+\Delta 4168\text{-}4907}$ by fusing a GFP to AAA5 and a spytag into the linker top2 domain. The GFP allowed us to anchor the construct to anti-GFP decorated cover slides and we covalently fused a spycatcher construct carrying the dynein microtubule binding domain into the linker top2 domain via the spytag-spycatcher interaction [25] (Fig. 5B). After the application of fluorescently labelled microtubules we were able to observe occasional events of directed microtubule sliding (Fig. 5C, Movies S3-S5) indicating that the remodelling of the linker top with respect to the AAA+ ring is able to produce mechanical force. The D/E rich region is largely dispensable and the MIDAS domain is not required for this force generation.

Taken together, these results suggest that the mechanical force produced by linker remodelling might be directly applied to the AAA+ ring docked MIDAS domain via the linker top2 domain to remove assembly factors from pre60S particles.

The Linker middle domain acts as a crucial hub for linker remodelling

Next we wanted to establish, which structural elements of the linker are crucial for its remodelling. In a previous study we had identified an α-helical extension of the linker middle domain that contacts the Rea1 AAA+ ring [18] (Fig. 6A). We speculated that this α-helical extension might participate in the communication of ATP induced conformational changes from the AAA+ ring into the linker to drive its remodelling [18]. In order to clarify its functional role, we deleted this α-helix and characterized linker remodelling in the presence of ATP by negative stain EM. Our analysis reveals that Rea1$_{\Delta 2916\text{-}2974}$ is able to sample states 1-6 (Fig. 6B). There is no evidence for state 7, which we would expect to detect under these nucleotide conditions (compare Fig. 1E), suggesting that this mutant is impaired in its ability to sample the linker states associated with ATP-hydrolysis. This conclusion is also supported by defects in the GFP-pre60S export assay (Fig. 6C) as well as non-viable spores in our tetrad dissection assay (Fig. 6D). Another prominent feature of the Rea1 linker middle domain is the globular extension that supports the U-shaped arrangement of the linker top [18] (Fig. 6A). Deleting the globular extension in the construct Rea1$_{\Delta 3072\text{-}3244}$ destabilizes the linker top and leads to partial degradation of Rea1 so that only the Rea1 AAA+ ring can be detected in our negative stain analysis (Supplementary figure 9). Consequently, the export of GFP labelled pre60S particles is compromised (Fig. 6D). Next, we screened for highly conserved amino-acid residues in the Rea1 linker. To this end we used the “ConSurf” server to plot a multiple sequence alignment onto the surface of the Rea1 linker. Although the general

conservation within the Rea1 linker domain is quite low, we nevertheless identified a highly conserved salt-bridge network, D2915-R2976-D3042, in close proximity to the α-helical extension of the linker middle domain (Fig. 6A). The disruption of this salt-bridge network by alanine mutations changed the remodelling pathway of the linker. While the region between the linker middle and stem domains still acts as pivot point for the swing of linker middle-top domains towards the AAA+ ring, Rea1$_{D2915A-R2976A-D3042A}$ did not show the rotation of the linker middle and top domain around the long linker axis that we consistently detected in all previous data sets (Fig. 6B, MovieS6). We also characterized Rea1$_{D2915A-R2976A-D3042A}$ by cryoEM in the presence of ATP. We were able to obtain three reconstructions at medium to low resolution (Fig 6.E and supplementary figure 10). As expected, the auto-inhibited state characterized by the straight, un-rotated linker, was the dominant class (conformation I.), and refined to a resolution sufficient to resolve secondary structure elements. In addition, we were able to resolve two alternative linker conformations of Rea1$_{D2915A-R2976A-D3042A}$ (conformations II. and III.) at a resolution allowing the docking of the linker stem-AAA+ ring rigid body as well as the linker middle-top rigid body. We attribute these differences in the final resolution mainly to the increased structural flexibility of conformations II. and III. As expected, conformations II. and III. were related by a swing of the linker top and middle domains towards the AAA+ ring without rotation around the long linker axis (Supplementary figure 11). These 3D cryoEM reconstructions confirm our initial assignment of the linker middle-stem region as pivot point for linker remodelling. We also characterized Rea1$_{D2915A-R2976A-D3042A}$ with our GFP-pre60S export and tetrad dissection assays and observe a defect in the pre60S export (Fig.6C) as well as a severe growth defect (Fig. 6D).

These results establish the linker middle domain as a critical hub for Rea1 linker remodelling. The α-helical extension is needed to fully sample all the states associated with ATP-hydrolysis suggesting it is indeed involved in communicating ATP-hydrolysis driven conformational changes from the AAA+ ring into the linker. The globular extension of the middle domain functions as a critical structural support for the architecture of the Rea1 linker. The conserved D2915-R2976-D3042 salt-bridge network is required for the rotation of the linker top-middle domain around the long linker axis during remodelling. Even though the long linker axis rotation is part of the intrinsic structural flexibility of the Rea1 linker and does not require ATP-hydrolysis, it nevertheless is of functional importance. The rotation is required to ensure the correct orientation of the linker top prior to its ATP-hydrolysis driven engagement with the AAA+ ring.

Discussion

The results presented here reveal the general principles of the Rea1 mechanism (Fig. 7), one of the largest and most complex ribosome maturation factors. We have demonstrated that the Rea1 linker

is a functionally important structural element that undergoes an elaborated series of remodelling events. We have identified eight distinct linker remodelling states illustrating the broad structural flexibility of the Rea1 linker. Two general aspects characterize and connect these remodelling events. The first aspect is the swing of the linker top and middle domains towards the AAA+ ring docked MIDAS domain with the region in-between the linker middle and stem domains acting as pivot point. The second aspect is the rotation of the linker top and middle domains around the long linker axis. A particularly interesting feature of this remodelling pathway is the occurrence of events that are part of the intrinsic structural flexibility of the linker like in the case of states 1 – 5. Even though these remodelling events do not depend on nucleotide binding or energy provided by ATP hydrolysis, they still play an important functional role. They ensure that linker top domains are in close proximity to the AAA+ ring and have the correct orientation prior to the ATP hydrolysis driven engagement with the AAA+ ring. The latter aspect is particularly highlighted by the inability of the $Rea1_{D2915A\text{-}R2976A\text{-}D3042A}$ mutant to rotate its linker (Fig. 6B) and the subsequent functional defect in the nuclear export of pre60S particles (Fig. 6C).

ATP hydrolysis is required to engage the rotated linker top domains with the AAA+ ring during states 6 – 8. The ultimate goal of the linker remodelling pathway is to bring the linker top 2 domain into contact with the AAA+ ring docked and substrate engaged MIDAS domain. We have demonstrated that Rea1 linker remodelling is able to produce mechanical force, which would allow the linker top 2 domain to pull on the substrate engaged MIDAS domain to remove assembly factors for pre60S particles. We consistently detected that the Rea1 linker states associated with ATP-hydrolysis are sampled only by a minority of particles in our data sets. One possible explanation could be that these states are simply transient and extremely short lived during the mechanochemical cycle of Rea1, so that even in the presence of slowly hydrolysable analogues like ATPγS no major enrichment occurs. Another possibility is that additional factors are required to further stabilize them such as protein/RNA interaction partners provided in the context of pre60S particle binding.

We have focused our analysis on the linker remodelling states that we consistently detected in our negative stain EM data sets. States 1 – 5 suggest that the swing of the linker towards the AAA+ ring and the rotation of the linker top are correlated events, i.e. the linker rotates as it swings towards the AAA+ ring. However, this correlation is not completely strict as in some of the data sets additional linker extended and intermediate states appeared suggesting that the linker can also swing without rotation or fully rotate before reaching the proximity of the AAA+ ring (supplementary figure 12). The occurrence of these states indicates that alternative pathways exist to remodel the linker from state 1 to state 5.

It is not clear why Rea1 would follow such an elaborate scheme to remove assembly factors from pre60S particles. One possibility is that states 1 – 5 constitute a sensing mechanism. After binding to pre60S particles has occurred, the intrinsic conformational flexibility represented by these states would allow the linker top to come close to the AAA+ ring – pre60S interface to probe if essential maturation events have occurred, before ATP-hydrolysis dependent linker remodelling proceeds to bring the linker top 2 domain in contact with the MIDAS domain to trigger assembly factor removal.

Currently, there are two mechanistic models for Rea1 functionality. Early structural studies on Rea1 favoured the linker remodelling hypothesis to remove assembly factors from pre60S particles [10], whereas more recently an alternative AAA+ ring model was suggested. In this model, ATP driven conformational changes in the AAA+ ring are directly communicated to the AAA+ ring docked and substrate engaged MIDAS domain to produce force for pre60S assembly factor removal [20, 23]. The latter model attributes a more passive role to the Rea1 linker suggesting it acts as a "fishing post" for the flexibly attached MIDAS domain and is not involved in force production [20]. The results presented here favour the linker remodelling hypothesis. Especially the data on the $Rea1_{\Delta 2916\text{-}2974}$ and $Rea1_{D2915A\text{-}R2976A\text{-}D3042A}$ mutants suggest that a potential AAA+ ring based force production for assembly factor removal is not essential to the Rea1 mechanism. Our structural characterization of these mutants clearly indicates that AAA+ ring and linker are well folded, but nevertheless they show severe functional defects. While these defects can be explained by the linker remodelling hypothesis, the AAA+ ring model would expect these mutants to be functional. Nevertheless, it is still possible that AAA+ ring based force production plays a supportive role in linker driven assembly factor removal.

Together with the motor protein dynein and the E3 ubiquitin ligase RNF213, Rea1 forms a special subclass within the AAA+ field. All these proteins have their six AAA+ modules concatenated into a single gene, whereas the hexameric AAA+ rings of the vast majority of AAA+ machines are formed by association of individual protomers. In the case of dynein and Rea1, ATP hydrolysis in the AAA+ ring drives the remodelling of an AAA+ ring linker extension, which in both cases correlates with the production of mechanical force. The dynein linker is with around 400 amino-acid residues much smaller than the Rea1 linker, which spans over around 1700 amino-acid residues, and there are no structural similarities between them. The dynein linker switches between a straight post-powerstroke and bent pre-powerstroke conformation [26] illustrating that the structural heterogeneity is much smaller compared to the Rea1 linker, which is able to adopt at least 9 different conformations (straight, extended linker conformations + states 1 – 8). These differences might be explained by the purpose of force production in dynein and Rea1. The processive movement along microtubules requires highly repetitive linker remodelling. In this context the switch between two remodelling states ensures efficient and fast force production. Rea1 on the other hand functions as a quality

control machine. The main task is not highly repetitive force production but rather a single force production event at a precisely controlled time point. In this context many linker remodelling steps offer the opportunity to integrate various signals from the pre60S environment to trigger assembly factor removal only when essential pre60S maturation events have occurred. The linker of the E3 ubiquitin ligase RNF213 is similar to the straight post-powerstroke dynein linker [27]. However, so far no alternative linker remodelling states have been reported for RNF213. It has been demonstrated that ATP binding to the AAA+ ring stimulates the ubiquitin ligase activity [28].

This study highlighted the general mechanistic principles of Rea1. Fully understanding the molecular basis of the Rea1 mechanism will require high resolution investigations on the various linker remodelling states. Especially the AAA+ ring engaged states will be of great interest as these are the ones associated with ATP hydrolysis and mechanical force production. The extreme low abundance of these states and the structural flexibility of the linker will make such investigations challenging.

Acknowledgement

We thank Andrew Carter for providing a plasmid harbouring the SRS-dynein MTBD construct. This work was supported by the collaborative ANR PRC grant “Rea1Com” to H.S. and A.H.

References

1. Thomson, E., S. Ferreira-Cerca, and E. Hurt, *Eukaryotic ribosome biogenesis at a glance.* J Cell Sci, 2013. **126**(Pt 21): p. 4815-21.
2. Kressler, D., E. Hurt, and J. Bassler, *Driving ribosome assembly.* Biochim Biophys Acta, 2010. **1803**(6): p. 673-83.
3. Harnpicharnchai, P., et al., *Composition and functional characterization of yeast 66S ribosome assembly intermediates.* Mol Cell, 2001. **8**(3): p. 505-15.
4. Venema, J. and D. Tollervey, *Ribosome synthesis in Saccharomyces cerevisiae.* Annu Rev Genet, 1999. **33**: p. 261-311.
5. Tang, L., et al., *Interactions among Ytm1, Erb1, and Nop7 required for assembly of the Nop7-subcomplex in yeast preribosomes.* Mol Biol Cell, 2008. **19**(7): p. 2844-56.
6. Sahasranaman, A., et al., *Assembly of Saccharomyces cerevisiae 60S ribosomal subunits: role of factors required for 27S pre-rRNA processing.* EMBO J, 2011. **30**(19): p. 4020-32.
7. Bassler, J., et al., *Identification of a 60S preribosomal particle that is closely linked to nuclear export.* Mol Cell, 2001. **8**(3): p. 517-29.
8. Bassler, J., et al., *The AAA-ATPase Rea1 drives removal of biogenesis factors during multiple stages of 60S ribosome assembly.* Mol Cell, 2010. **38**(5): p. 712-21.
9. Nissan, T.A., et al., *A pre-ribosome with a tadpole-like structure functions in ATP-dependent maturation of 60S subunits.* Mol Cell, 2004. **15**(2): p. 295-301.
10. Ulbrich, C., et al., *Mechanochemical removal of ribosome biogenesis factors from nascent 60S ribosomal subunits.* Cell, 2009. **138**(5): p. 911-22.
11. Bassler, J., et al., *A network of assembly factors is involved in remodeling rRNA elements during preribosome maturation.* J Cell Biol, 2014. **207**(4): p. 481-98.
12. Bradatsch, B., et al., *Structure of the pre-60S ribosomal subunit with nuclear export factor Arx1 bound at the exit tunnel.* Nat Struct Mol Biol, 2012. **19**(12): p. 1234-41.

13. Leidig, C., et al., *60S ribosome biogenesis requires rotation of the 5S ribonucleoprotein particle.* Nat Commun, 2014. **5**: p. 3491.
14. Barrio-Garcia, C., et al., *Architecture of the Rix1-Rea1 checkpoint machinery during pre-60S-ribosome remodeling.* Nat Struct Mol Biol, 2016. **23**(1): p. 37-44.
15. Matsuo, Y., et al., *Coupled GTPase and remodelling ATPase activities form a checkpoint for ribosome export.* Nature, 2014. **505**(7481): p. 112-6.
16. Garbarino, J.E. and I.R. Gibbons, *Expression and genomic analysis of midasin, a novel and highly conserved AAA protein distantly related to dynein.* BMC Genomics, 2002. **3**: p. 18.
17. Winzeler, E.A., et al., *Functional characterization of the S. cerevisiae genome by gene deletion and parallel analysis.* Science, 1999. **285**(5429): p. 901-6.
18. Sosnowski, P., et al., *The CryoEM structure of the Saccharomyces cerevisiae ribosome maturation factor Rea1.* Elife, 2018. **7**.
19. Kater, L., et al., *Construction of the Central Protuberance and L1 Stalk during 60S Subunit Biogenesis.* Mol Cell, 2020. **79**(4): p. 615-628 e5.
20. Chen, Z., et al., *Structural Insights into Mdn1, an Essential AAA Protein Required for Ribosome Biogenesis.* Cell, 2018. **175**(3): p. 822-834 e18.
21. Ahmed, Y.L., et al., *Crystal structures of Rea1-MIDAS bound to its ribosome assembly factor ligands resembling integrin-ligand-type complexes.* Nat Commun, 2019. **10**(1): p. 3050.
22. Mickolajczyk, K.J., et al., *The MIDAS domain of AAA mechanoenzyme Mdn1 forms catch bonds with two different substrates.* Elife, 2022. **11**.
23. Mickolajczyk, K.J., et al., *Long-range intramolecular allostery and regulation in the dynein-like AAA protein Mdn1.* Proc Natl Acad Sci U S A, 2020. **117**(31): p. 18459-18469.
24. Ripstein, Z.A., et al., *Structure of a AAA+ unfoldase in the process of unfolding substrate.* Elife, 2017. **6**.
25. Zakeri, B., et al., *Peptide tag forming a rapid covalent bond to a protein, through engineering a bacterial adhesin.* Proc Natl Acad Sci U S A, 2012. **109**(12): p. E690-7.
26. Burgess, S.A., et al., *Dynein structure and power stroke.* Nature, 2003. **421**(6924): p. 715-8.
27. Ahel, J., et al., *Moyamoya disease factor RNF213 is a giant E3 ligase with a dynein-like core and a distinct ubiquitin-transfer mechanism.* Elife, 2020. **9**.
28. Ahel, J., et al., *E3 ubiquitin ligase RNF213 employs a non-canonical zinc finger active site and is allosterically regulated by ATP.* bioRxiv, doi: https://doi.org/10.1101/2021.05.10.443411

Figure 1

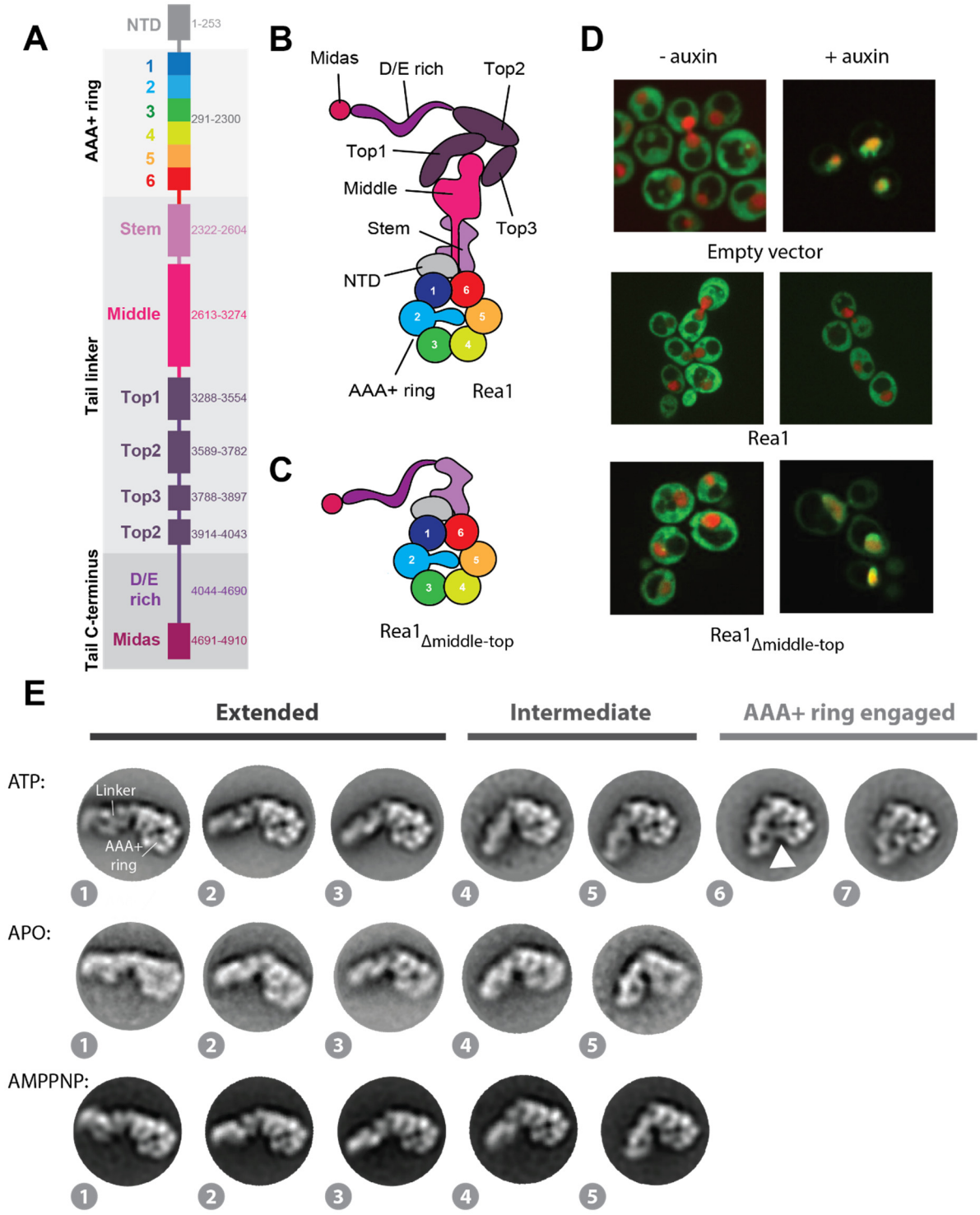

Figure 1: The Rea1 linker is a functionally important structural element and shows nucleotide independent as well as nucleotide dependent remodelling. A. Domain organization of Rea1. **B.** Schematic cartoon representation of Rea1. **C.** Schematic cartoon representation of a construct lacking the linker middle and top domains. The flexible D/E rich region with the substrate binding MIDAS domain are directly fused to the linker stem domain. **D.** Yeast nuclear export assay of pre-ribosomal particles. The pre-ribosomal particle marker Rpl25 is fused to GFP. Histone-cherry marks the nucleus. The endogenous Rea1 is under the control of the auxin degron system. Upper panels: The addition of

auxin leads to the accumulation of GFP fluorescence in the nucleus indicating a pre60S nuclear export defect due to degraded endogenous Rea1. Middle panels: The export defect can be rescued by a plasmid harbouring a wt Rea1 copy. Lower panels: Providing a plasmid harbouring the construct in C. does not rescue the export defect, suggesting the linker middle and top domains are functionally important. **E.** Negative stain 2D classes representing AAA+ ring top views of wt Rea1 in the presence of ATP, absence of nucleotide as well as in the presence of AMPPNP. States 1 – 5 represent the extended and intermediate linker conformations, which do not require nucleotide. In contrast to states 1 – 5, the AAA+ ring engaged states 6 and 7 require ATP hydrolysis. The white arrow head highlights a connection between the linker top and the AAA+ ring.

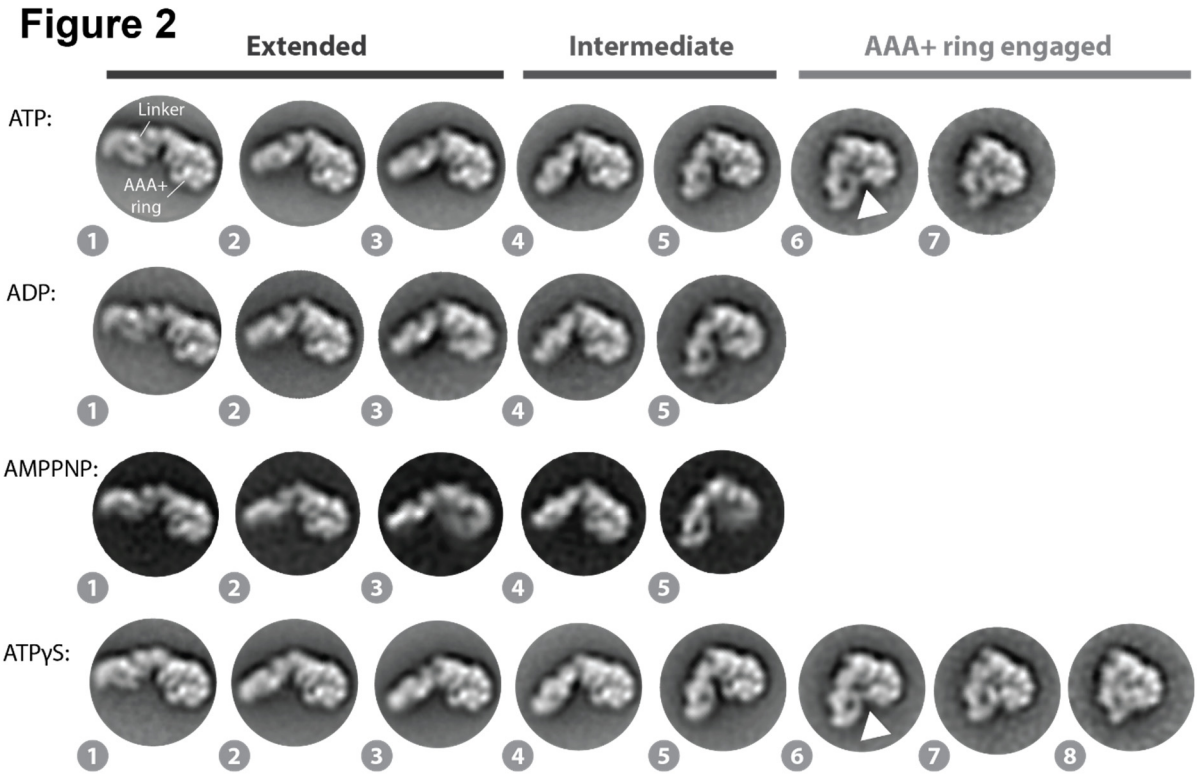

Figure 2: Linker remodelling in the Rea1ΔAAA2H2α mutant. The analysis of the ATP, ADP, AMPPNP and ATPγS data sets indicates that linker remodelling in Rea1ΔAAA2H2α is highly similar to linker remodelling in Rea1 wt. Like in the case of Rea1 wt, ATP-hydrolysis is required to engage the linker with the AAA+ ring. Unlike Rea1 wt, the Rea1ΔAAA2H2α mutant is able to sample state 8 in the presence of the slowly hydrolysable ATP analogue ATPγS. The white arrow head highlights a connection between the linker top and the AAA+ ring.

Figure 3

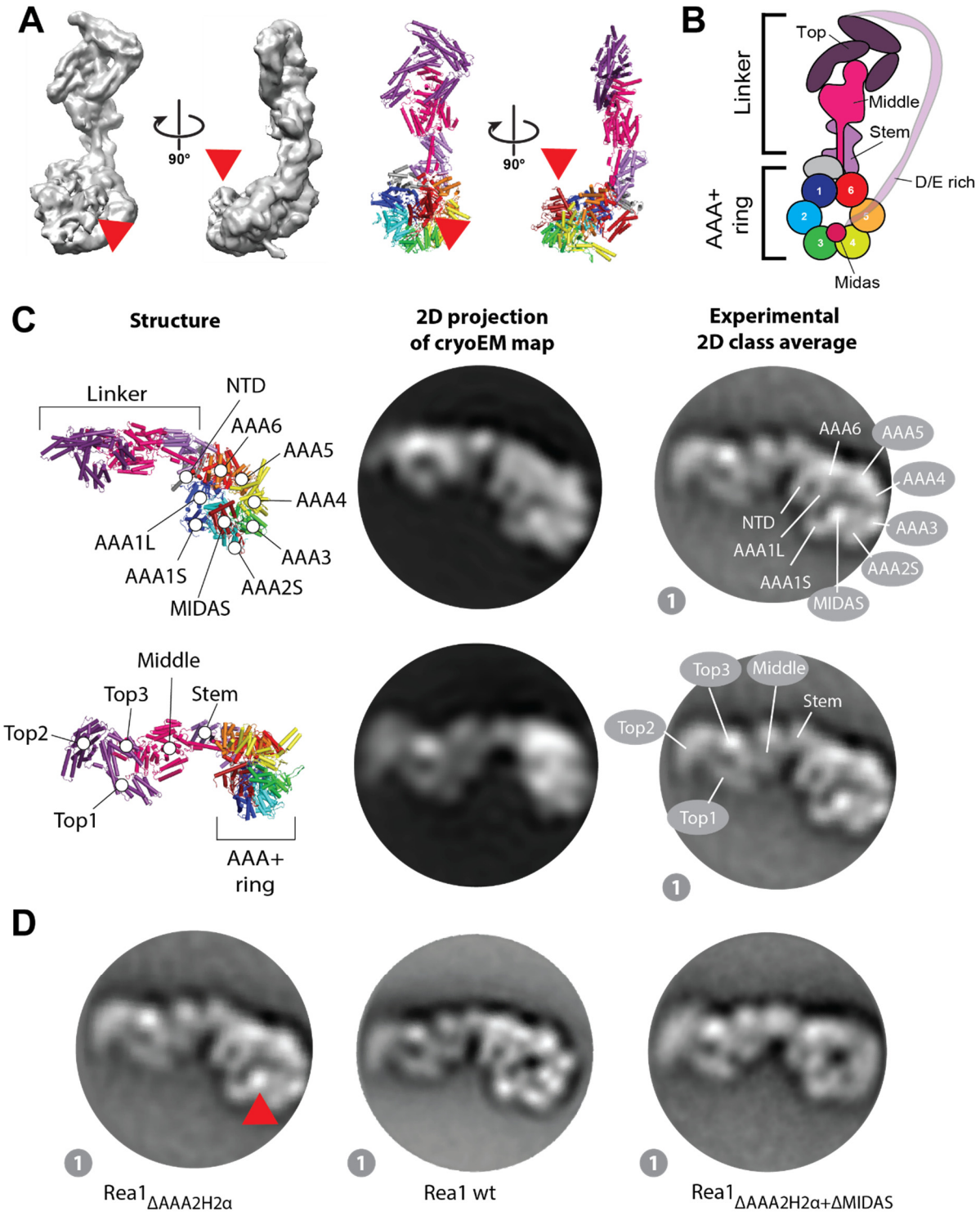

Figure 3: Domain assignments in negative stain 2D class averages of Rea1ΔAAA2H2α. A. CryoEM map (left panels) and cartoon representation (right panels) of Rea1ΔAAA2H2α in the presence of ATPγS. The red arrow heads highlight the AAA+ docked MIDAS domain. **B.** Schematic cartoon of the structure in A. The α-helical extension of AAA2 normally occupying the centre of the pore (compare Figure 1B) has been deleted, which allows the MIDAS domain to dock onto the AAA+ ring. The D/E rich region connecting the MIDAS domain to the linker top is flexible and not visible in the structure. **C.** Upper

panels: A 2D projection of the cryoEM map in A. shows a good match for the AAA+ ring region in the state 1 negative stain 2D class average. The projection allows the assignment of the NTD, AAA1 – AAA6, and the MIDAS domain. In contrast to the AAA+ ring region, the linker adopts a different conformation from the one seen in state 1. Lower panels: With a different 2D projection of the cryoEM map in A. a good match for the linker region in the state 1 negative stain 2D class average can be produced allowing the assignment of the linker top1, top2 and top3 domains as well as the linker middle domain. The AAA+ ring does not match up with the AAA+ ring in the state 1 negative stain 2D class average. This mismatch indicates that – compared to the cryoEM structure in A. - the linker in state 1 has moved with respect to the AAA+ ring. **D.** The assignment of the MIDAS domain in state 1 of Rea1ΔAAA2H2α (red arrow head, left panel) is further supported by comparisons with state 1 of Rea1 wt, where the MIDAS domain is absent (middle panel) as well as analysis of the Rea1ΔAAA2H2α+ΔMIDAS double mutant.

Figure 4

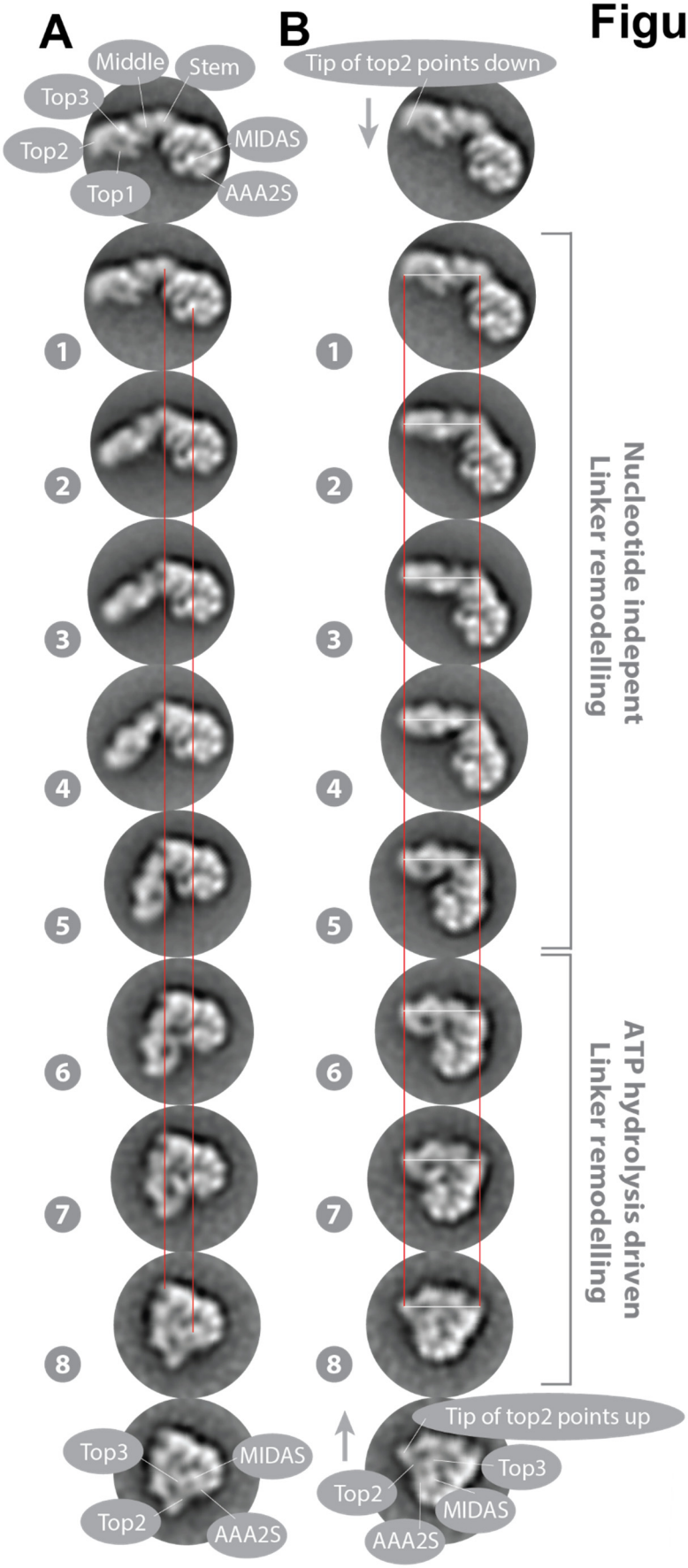

Figure 4: The Rea1 linker pivots and rotates during remodelling. A. States 1 – 8 of Rea1ΔAAA2H2α ATPγS aligned on the linker stem and MIDAS domains (red lines). The linker middle and top domains swing towards the AAA+ docked MIDAS domain (compare also movie S1). The region between the linker stem and middle domains acts as pivot point. Compare also movie S1. **B.** States 1 – 8 of Rea1ΔAAA2H2α ATPγS aligned on long linker axis (tip of linker top2 domain and linker stem domain, white and red lines). The linker middle and top domains rotate during the pivot swing (compare also movie S2). The tip of the linker top2 domain points downwards in state 1 (grey arrow) but upwards in state 8 (grey arrow) highlighting the rotation. In the final linker remodelling conformation, state 8, the linker top2 and top3 domains, AAA2S and the MIDAS domain are in close proximity. States 1 -5 were also observed under APO conditions (compare Figure 1E) indicating that large parts of the linker swing and the linker rotation are nucleotide independent and are part of the intrinsic conformational flexibility of the linker. The engagement of the rotated linker with the AAA+ ring during states 6 – 8 requires ATP hydrolysis.

Figure 5

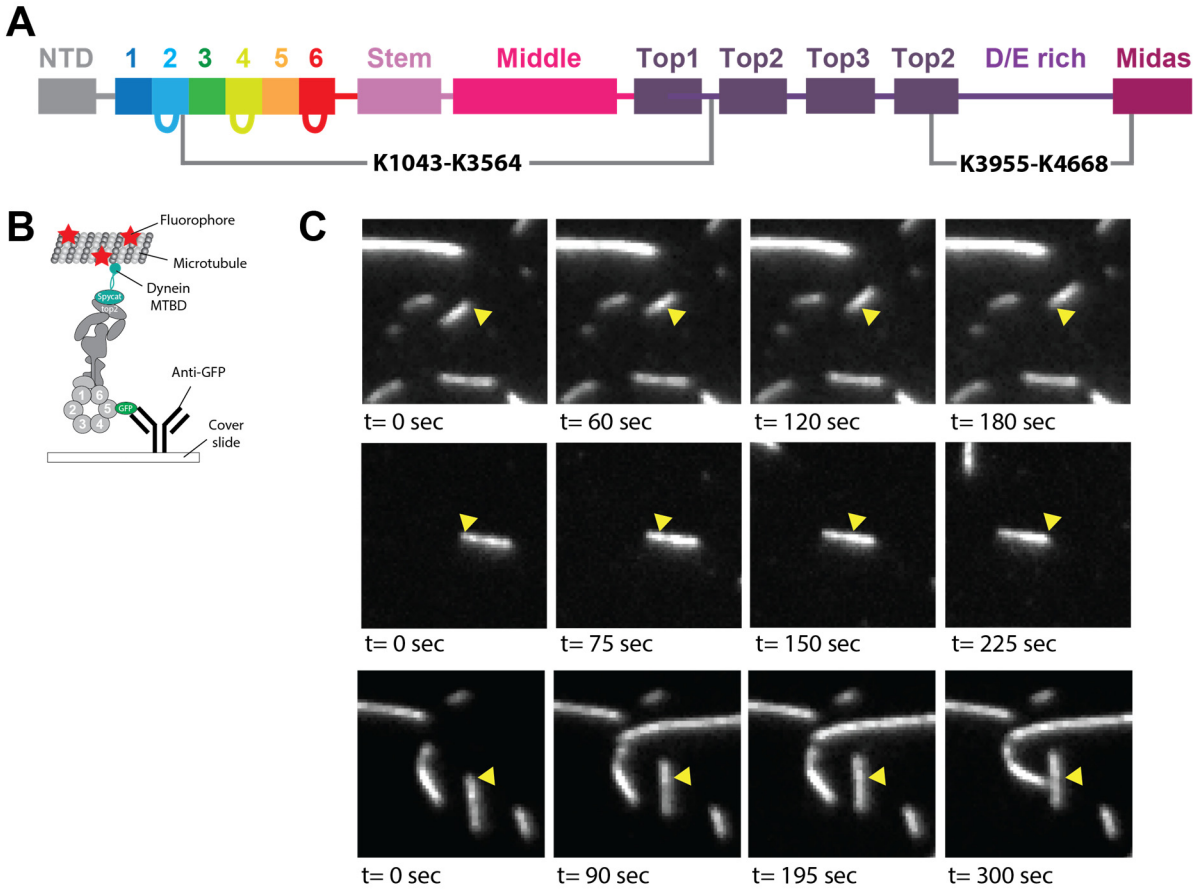

Figure 5: The linker top is able to interact with the MIDAS domain and linker remodelling is a force producing event. A. Two crosslinks supporting state 8 detected in Rea1ΔAAA2H2α in the presence of ATPγS. The K3955-K4668 crosslink indicates a direct interaction between the linker top2 domain and the MIDAS domain. The K1043-K3564 crosslink suggests proximity between the linker top2 domain and AAA2S, which is consistent with our domain assignment in state 8 (compare Figure 4). **B**. We carried out microtubule gliding assays with a Rea1ΔAAA2H2α construct to provide evidence that Rea1 linker remodelling produces force. The dynein microtubule binding domain (cyan) was fused to the linker top2 domain using the spycatcher/spytag approach and GFP to AAA5. The construct was anchored to a cover slide via GFP-antibodies and fluorescently labelled microtubules we applied. **C**. Three examples of gliding microtubules. The yellow arrow heads mark the position of the microtubule at the beginning of the movie (also compare movies S3-S5). The microtubule gliding events suggest that the remodelling of the linker with respect to the AAA+ ring is able to produce mechanical force.

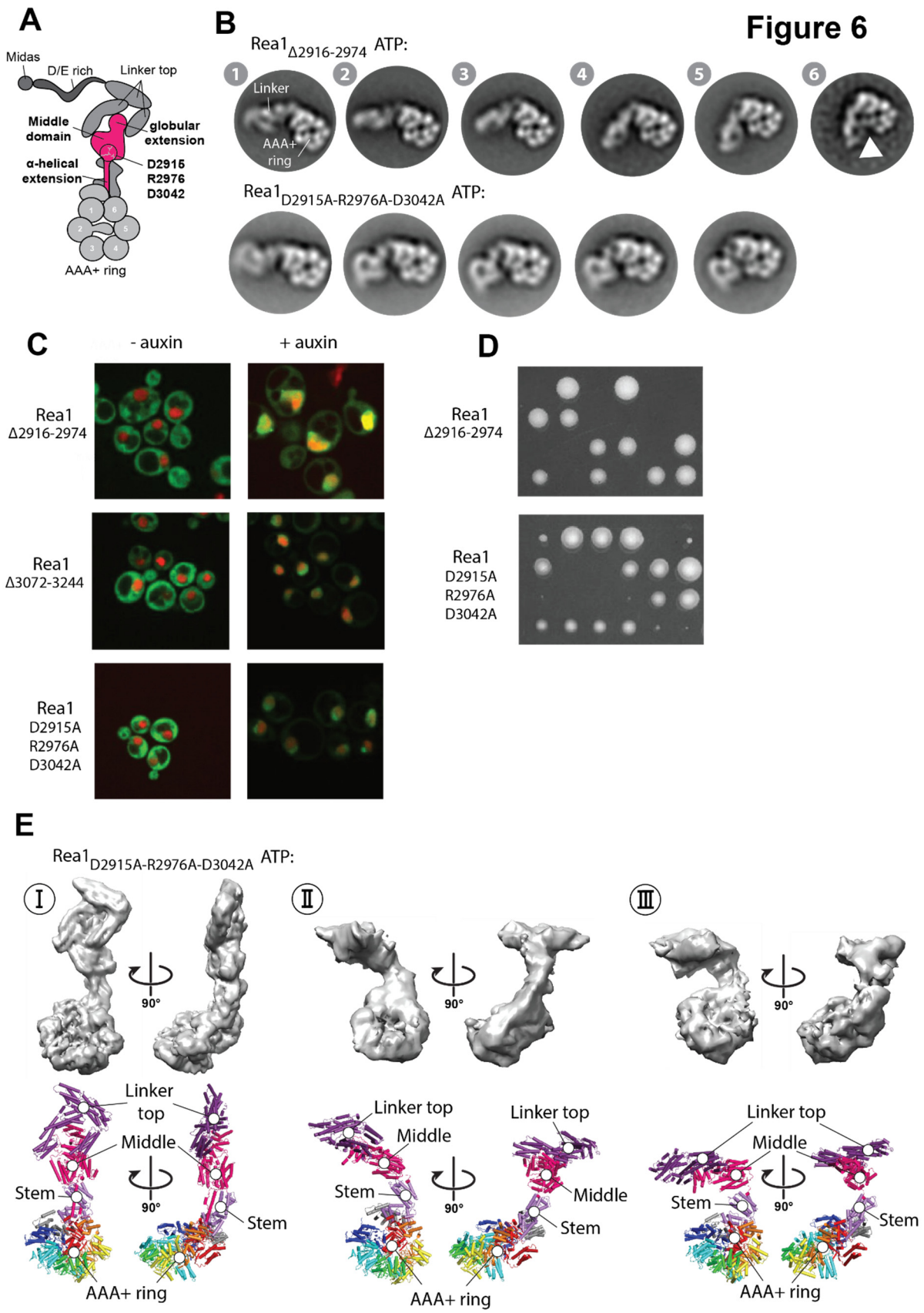

Figure 6: The linker middle domain has essential functions during linker remodelling. A. Schematic representation of three structural elements in the linker middle domain. The α-helical extension (aa 2916-2974), the globular extension (aa 3072-3244) and the highly conserved salt-bridge network

D2915-R2976-D3042. **B.** Deleting the α-helical extension or disrupting the D2915-R2976-D3042 salt-bridge network results in altered linker remodelling pathways. Deleting the α-helical extension prevents the sampling of state 7. The disruption of the D2915-R2976-D3042 still allows the linker swing towards the AAA+ ring but prevents the rotation of the linker middle and top domains around the long linker axis as well as the subsequent engagement with the AAA+ ring (compare also movie S6). Deleting the globular extension leads to the truncation of the whole linker (compare also supplementary figure 9) indicating that it serves a critical role for the stability of the linker. **C.** Deleting the α-helical or globular extension or disrupting the D2915-R2976-D3042 salt-bridge network leads to nuclear pre60S particle export defects. **D.** The critical functional role of the α-helical extension and the D2915-R2976-D3042 salt-bridge network was also confirmed in yeast tetrad dissection assays. **E.** Three cryoEM structures of the $Rea1_{D2915A\text{-}R2976A\text{-}D3042A}$ mutant in the presence of ATP. The linker conformation I is highly similar to the linker conformation of Rea1ΔAAA2H2α ATPγS (compare Figure A). In Conformations II and III the linker middle and top domains have swung towards the AAA+ ring. The region between the linker middle and stem domain acts as pivot point.

Figure 7

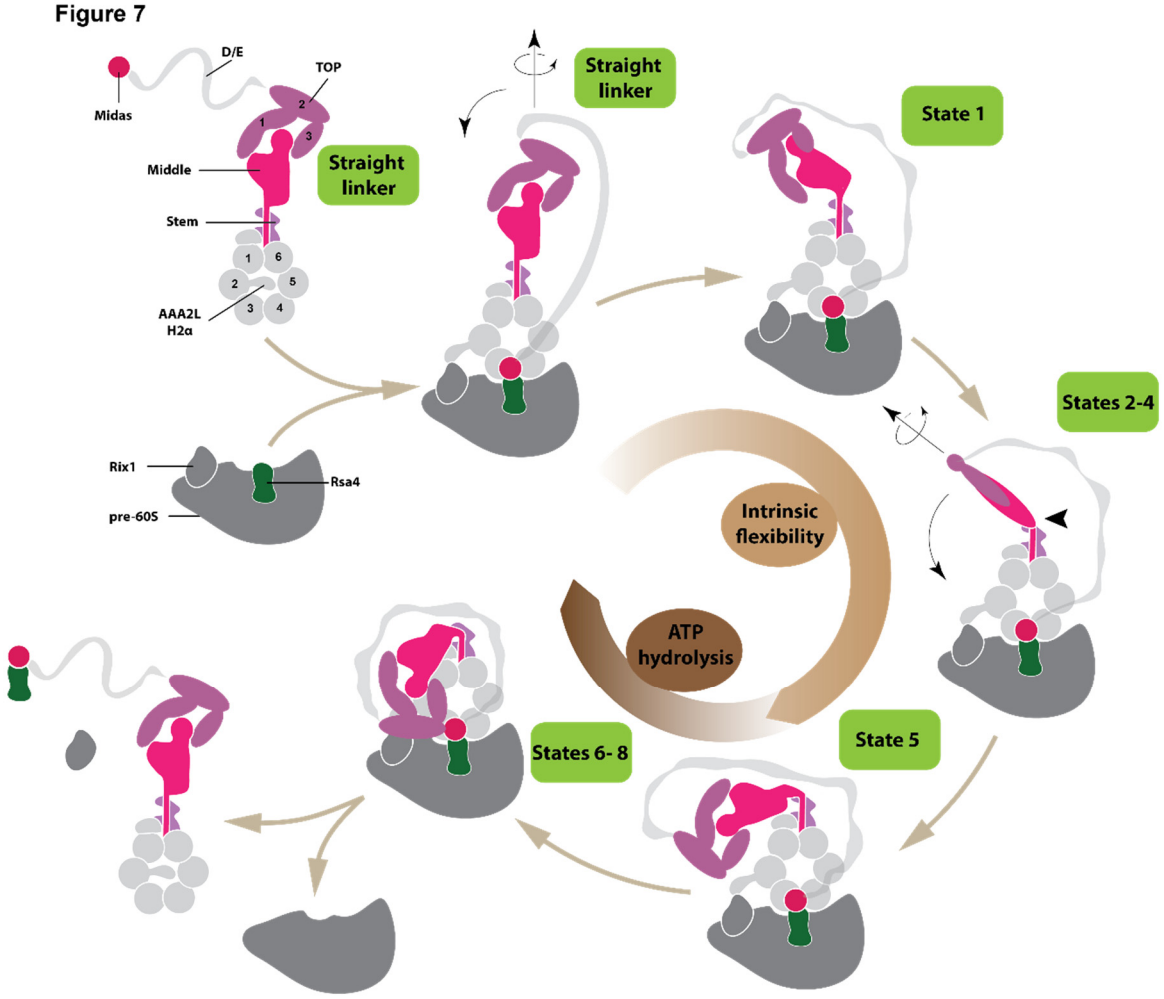

Figure 7: Model for the Rea1 mechanism. Rea1 in the absence of pre60S particles exists in an autoinhibited form with the AAA2H2α insert occupying the central pore of the AAA+ ring and the linker in the straight conformation. The binding of Rea1 to pre60S particles relocates AAA2H2α towards the pre60S particles which allows the MIDAS domain to dock onto the AAA+ ring to engage with its assembly factor substrate (here Rsa4). The linker remains in the straight conformation. The linker subsequently rotates and pivots towards the plane of the AAA+ ring to reach state 1. From here the linker middle and top domains rotate around the long linker axis and swing towards the AAA+ ring. The region between the linker middle and stem domains acts as pivot point. In state 5, the linker middle and top domains are fully rotated and in close proximity to the AAA+ ring. In states 6-8, the linker top engages with the AAA+ ring and in the final remodelling step state 8 the linker top2 domain interacts with the MIDAS domain to allow the transmission of force for assembly factor removal. Up to state, the linker remodelling is nucleotide independent and driven by the intrinsic conformational flexibility of the linker. States 6 – 8 require ATP hydrolysis.

Supplementary figure 1

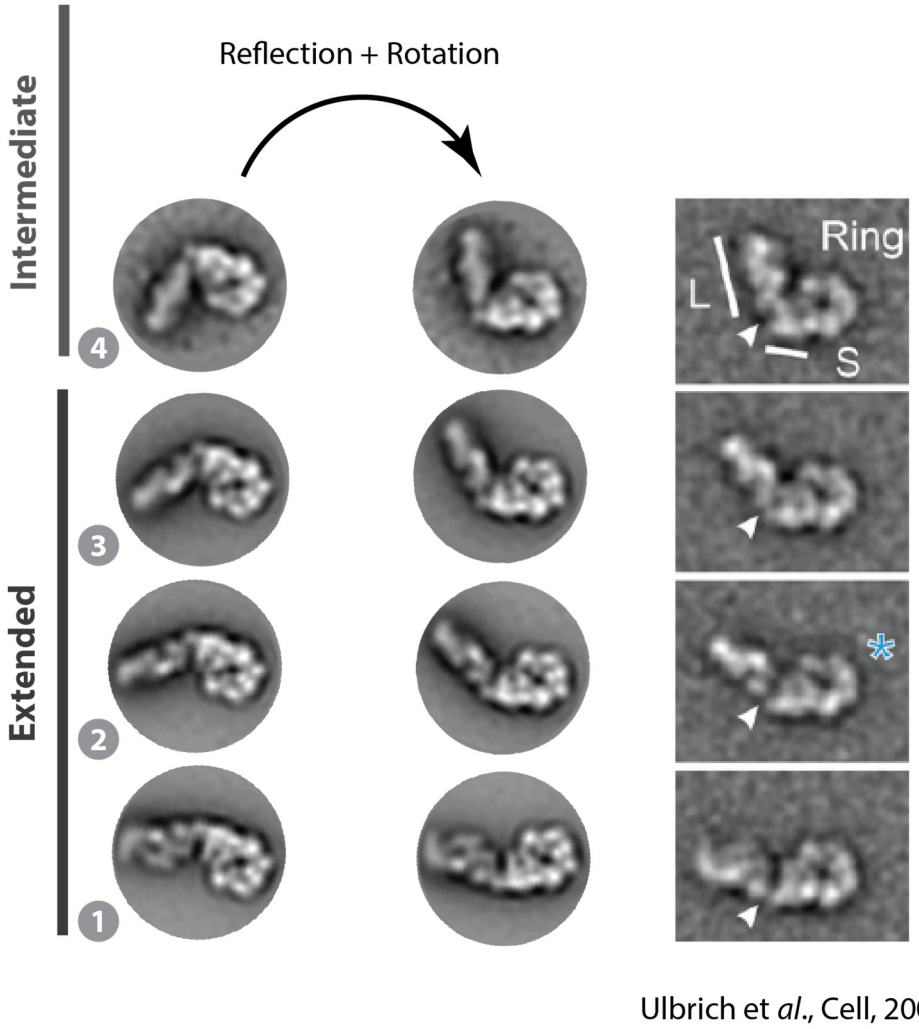

Ulbrich et *al*., Cell, 2009

Supplementary figure 1: Comparison of 2D classes with published data. States 1 -4 are similar to 2D classes published by Ulbrich et al.

Supplementary figure 2

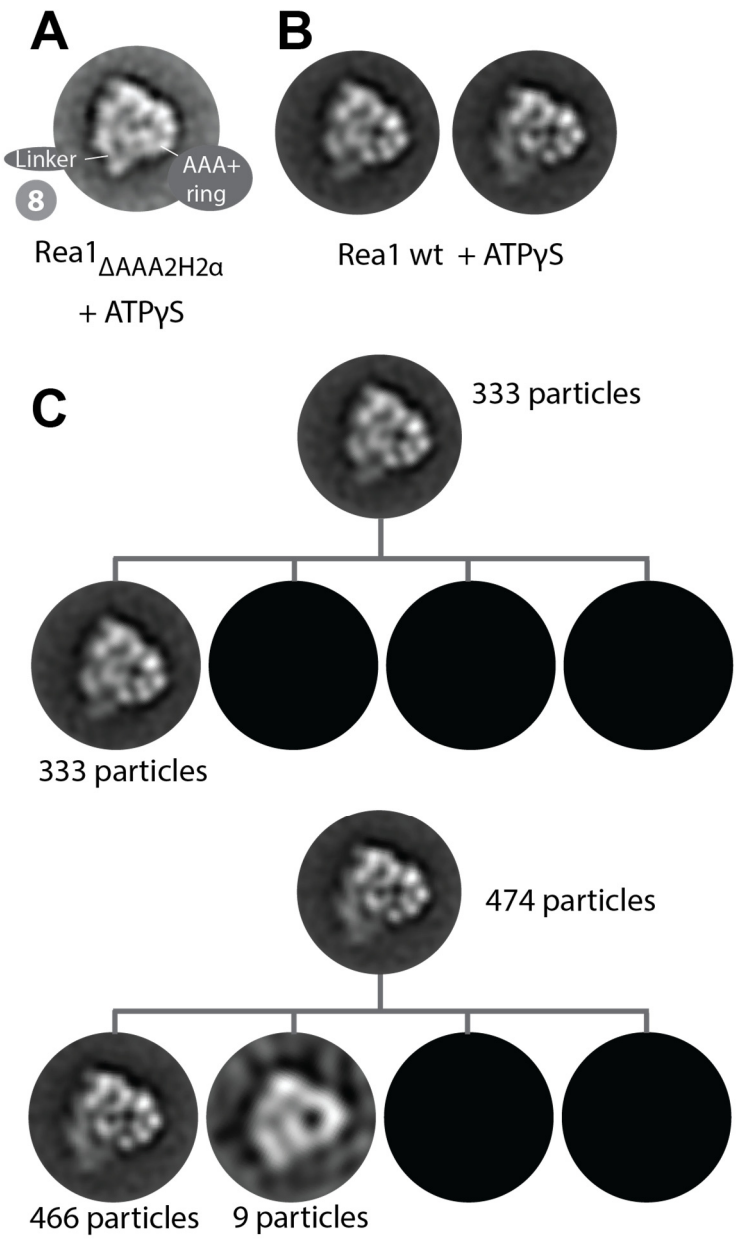

Supplementary figure 2: Linker remodelling state 8 is not stable in Rea1 wt. A. State 8 as observed in Rea1ΔAAA2H2α in the presence of ATPγS. **B.** Two 2D class averages obtained from a Rea1 wt ATPγS data set. The two 2D classes are similar to state 8 of Rea1ΔAAA2H2α, but thin stain for the linker tip (left) or the complete linker (right) indicates increased structural flexibility. **C.** The increased structural flexibility of the linker in B. might be due to a mixture of well-folded state 8 particles and partially or completely unfolded particles. To rule out this possibility, we re-classified the particles in B. into 4 sub-classes. The sub-classification brings back the original 2D classes conforming that the linker in these classes is too flexible to stably sample state 8.

Supplementary figure 3

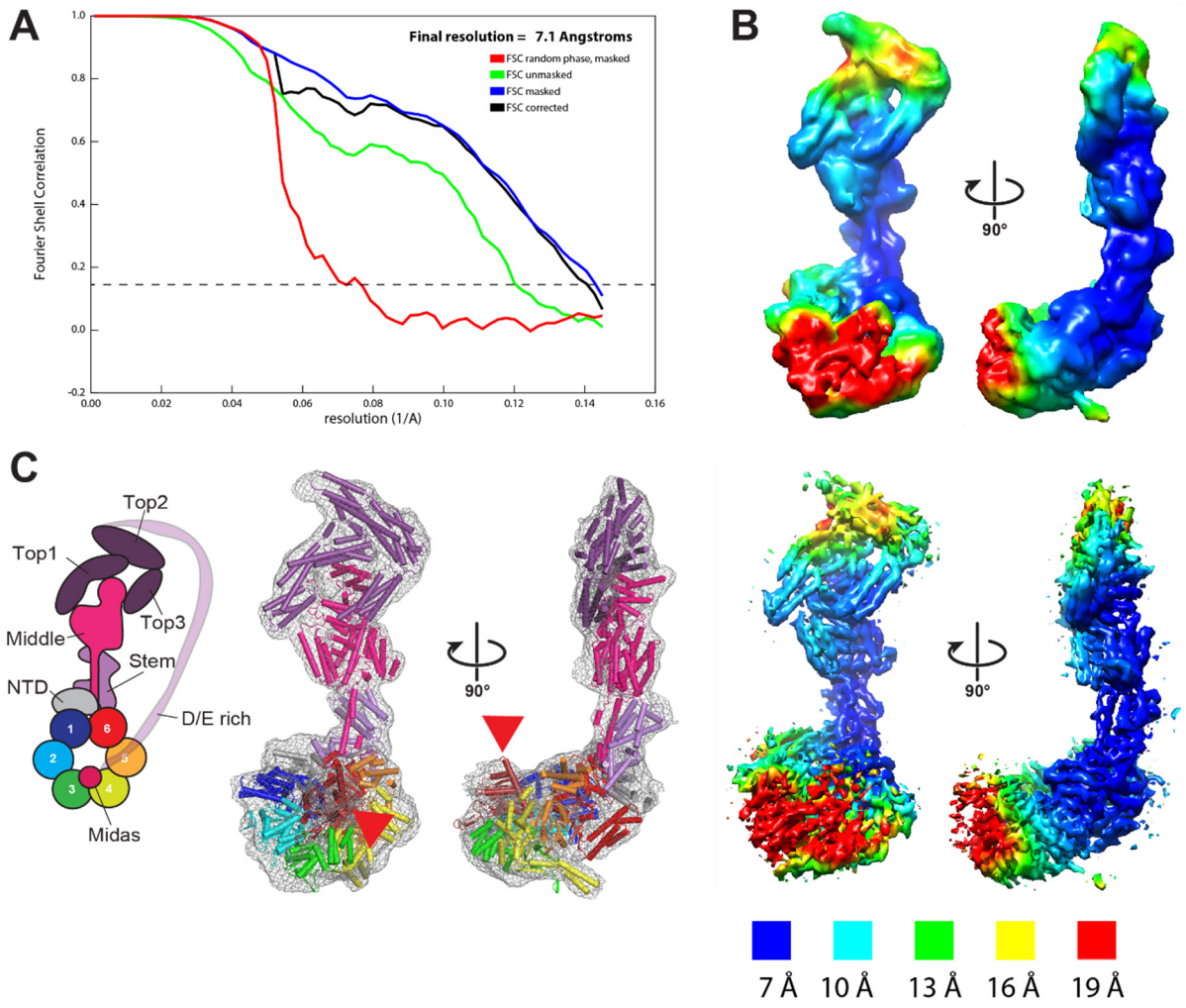

Supplementary figure 3: Overall quality of the Rea1ΔAAA2H2α ATPγS cryoEM map. A. Fourier shell correlation (FSC) plot for half-maps of the 3D reconstruction. The 0.143 FSC criteria is indicated as horizontal dashed line. The final overall resolution is 7.1 Å. **B.** Local resolution map, upper panels: unsharpened map, lower panels: B-factor sharpened map Secondary structure elements can be identified. **C.** Schematic cartoon representation of structure (left) and match of structure in map (right). Red arrow heads highlight the AAA+ ring docked MIDAS domain.

Supplementary figure 4

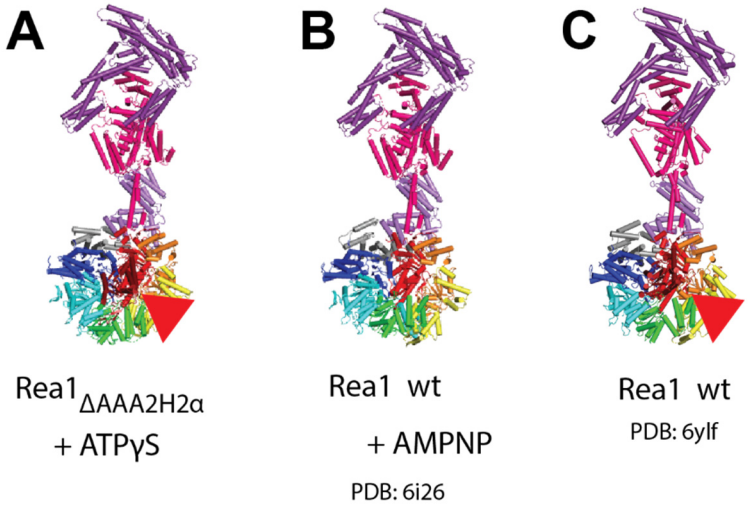

Supplementary figure 4: Comparison of the straight linker in Rea1ΔAAA2H2α ATPγS with previously published Rea1 cryoEM structures. A. Straight linker in Rea1ΔAAA2H2α ATPγS structure (this study). **B.** Rea1 wt in the presence of AMPNP (Sosnowski et al., 2018). **C.** Rea1 wt bound to a pre60S particle (Kater et al., 2020). In all structures the linker adopts the identical straight conformation. Red arrow heads highlight the AAA+ docked MIDAS domain.

Supplementary figure 5

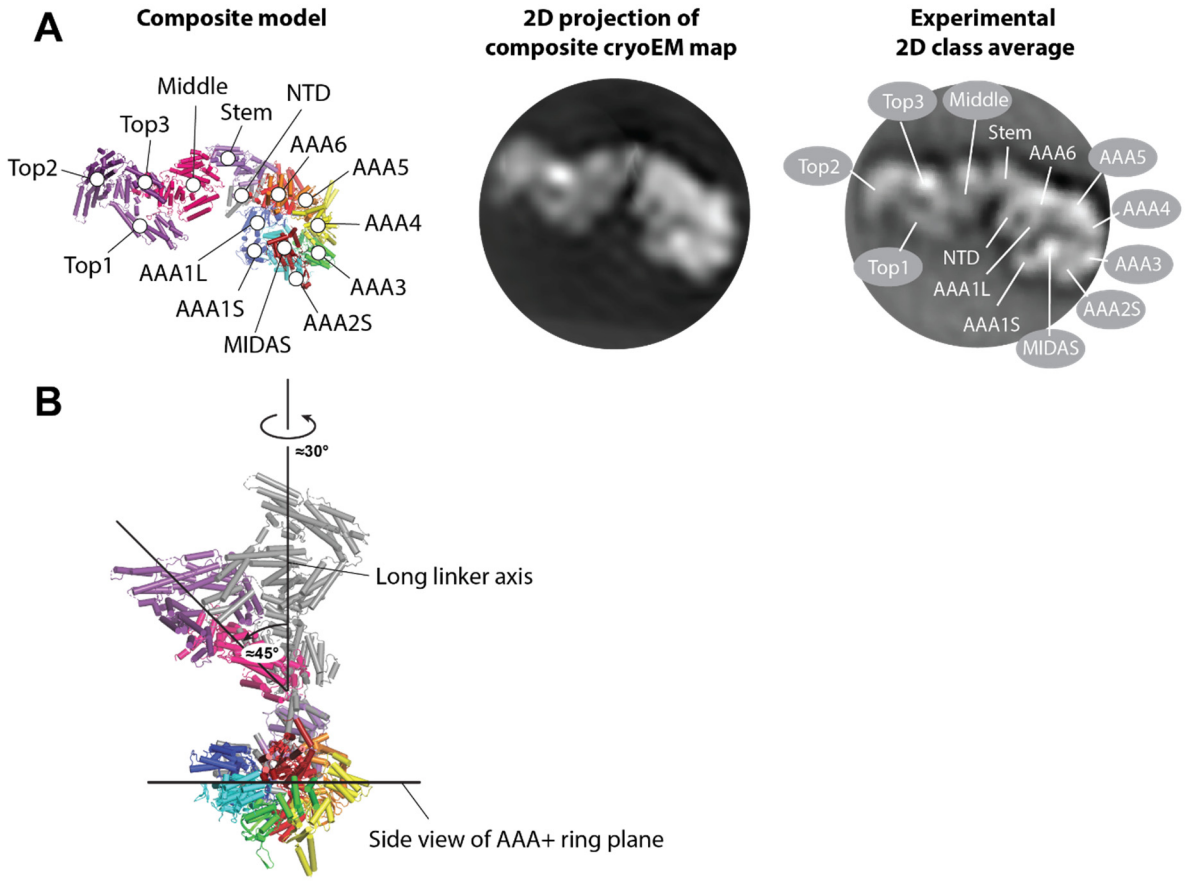

Supplementary figure 5: The linker in state 1 has moved with respect to the AAA+ ring compared to the straight linker conformation in Rea1ΔAAA2H2α ATPγS. A. Combining the AAA+ ring map in the orientation used to assign the AAA+ sub-domains in state 1 with the linker map in the orientation used to assign linker sub-domains in state 1 allowed us to create structural composite model for state 1. **B.** Aligning the AAA+ ring of this composite model with the AAA+ ring in Rea1ΔAAA2H2α ATPγS structure reveals that the linker has rotated by ≈ 30˚ and swung by ≈ 45˚ towards the AAA+ ring plane. Straight linker of the Rea1ΔAAA2H2α ATPγS structure is shown in grey.

Supplementary figure 6

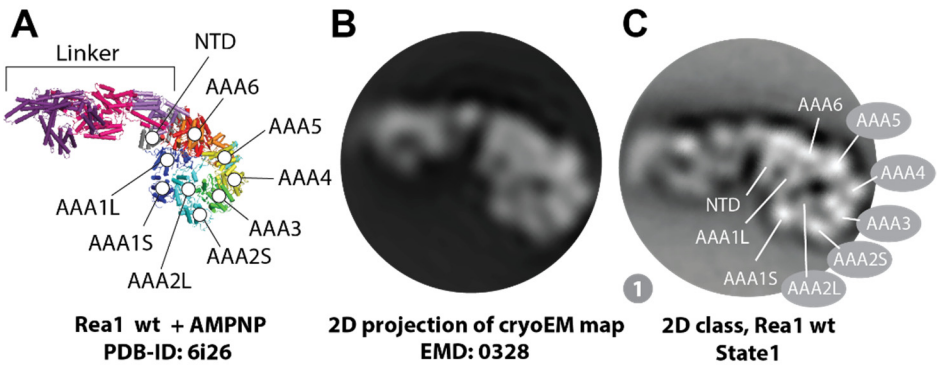

Rea1 wt + AMPNP
PDB-ID: 6i26

2D projection of cryoEM map
EMD: 0328

2D class, Rea1 wt
State1

Supplementary figure 6: The AAA+ ring in the 2D class averages of Rea1 wt does not harbour a docked MIDAS domain. A. Structure of Rea1 wt in the presence of AMPPNP (Sosnowski et al., 2018). The AAA+ ring does not feature a docked MIDAS domain **B.** 2D projection of the corresponding cryoEM map of A. **C.** The AAA+ ring in the 2D class averages of Rea1 wt (here state 1 as example) matches well with the projection in B. suggesting the MIDAS domain is not docked onto the AAA+ ring.

Supplementary figure 7

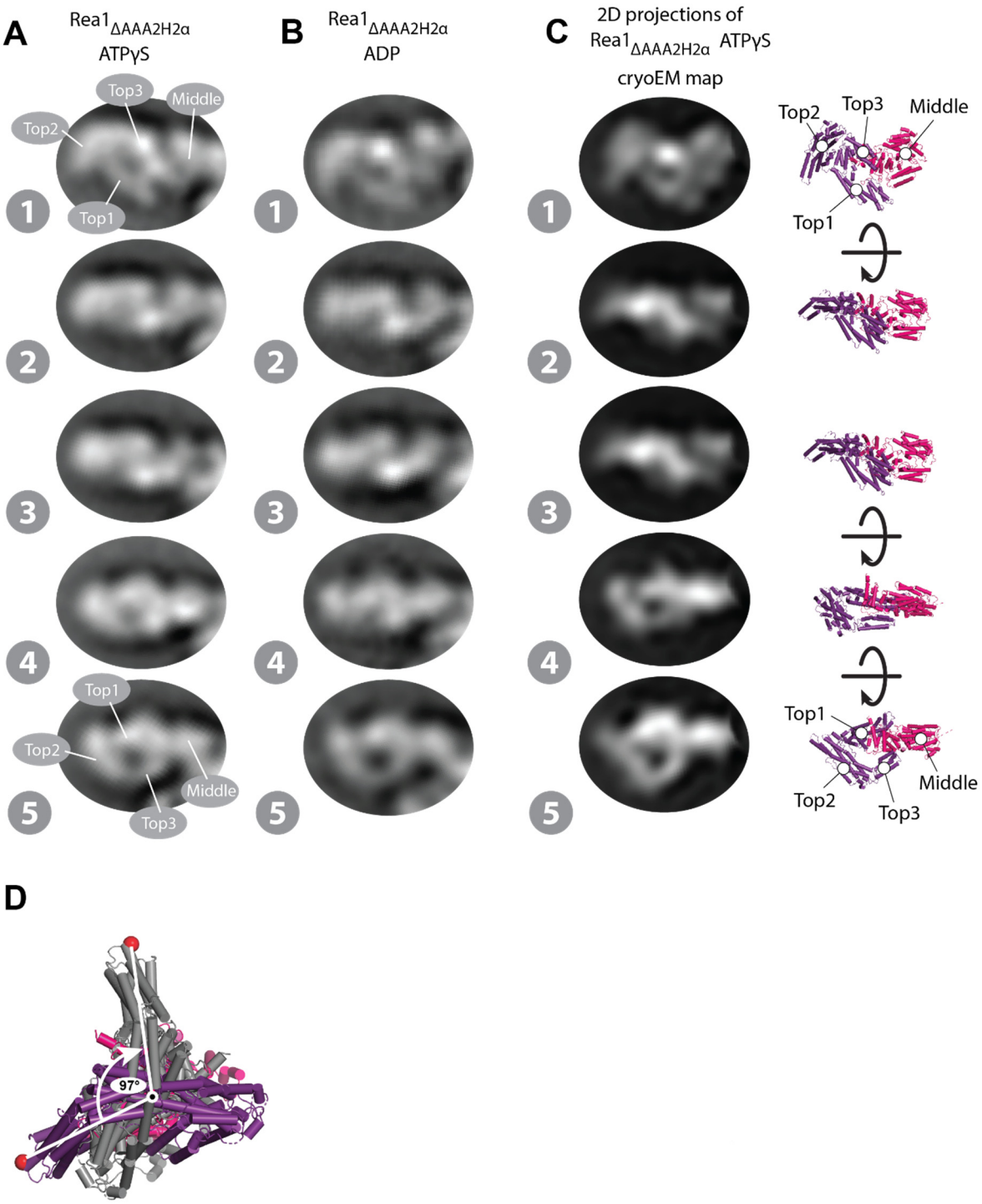

Supplementary figure 7: The linker top and middle domains rotate during linker remodelling. A. Enlarged views of linker region in states 1 – 5 of Rea1ΔAAA2H2α ATPγS. **B.** Enlarged views of linker region in states 1 – 5 of Rea1ΔAAA2H2α ADP. **C.** Left panels: Series of 2D projections of the linker middle-top part of the Rea1ΔAAA2H2α ATPγS cryoEM map rotated around the long linker axis. Right panels: corresponding structures. The rotation of the linker in A. and B. can be approximated by a rigid-body rotation of the linker middle and top domains around the long linker axis. Additional internal rearrangements of the linker middle and top domains with respect to each other cannot be excluded. **D.** Aligning states 1 (color coded) and 5 (grey) of C. on the long linker axis indicates a total rotation

angle of ≈ 100˚. Equivalent Cα atoms are shown as red spheres. The long linker axis (black dot) is perpendicular to the paper plane.

Supplementary figure 8

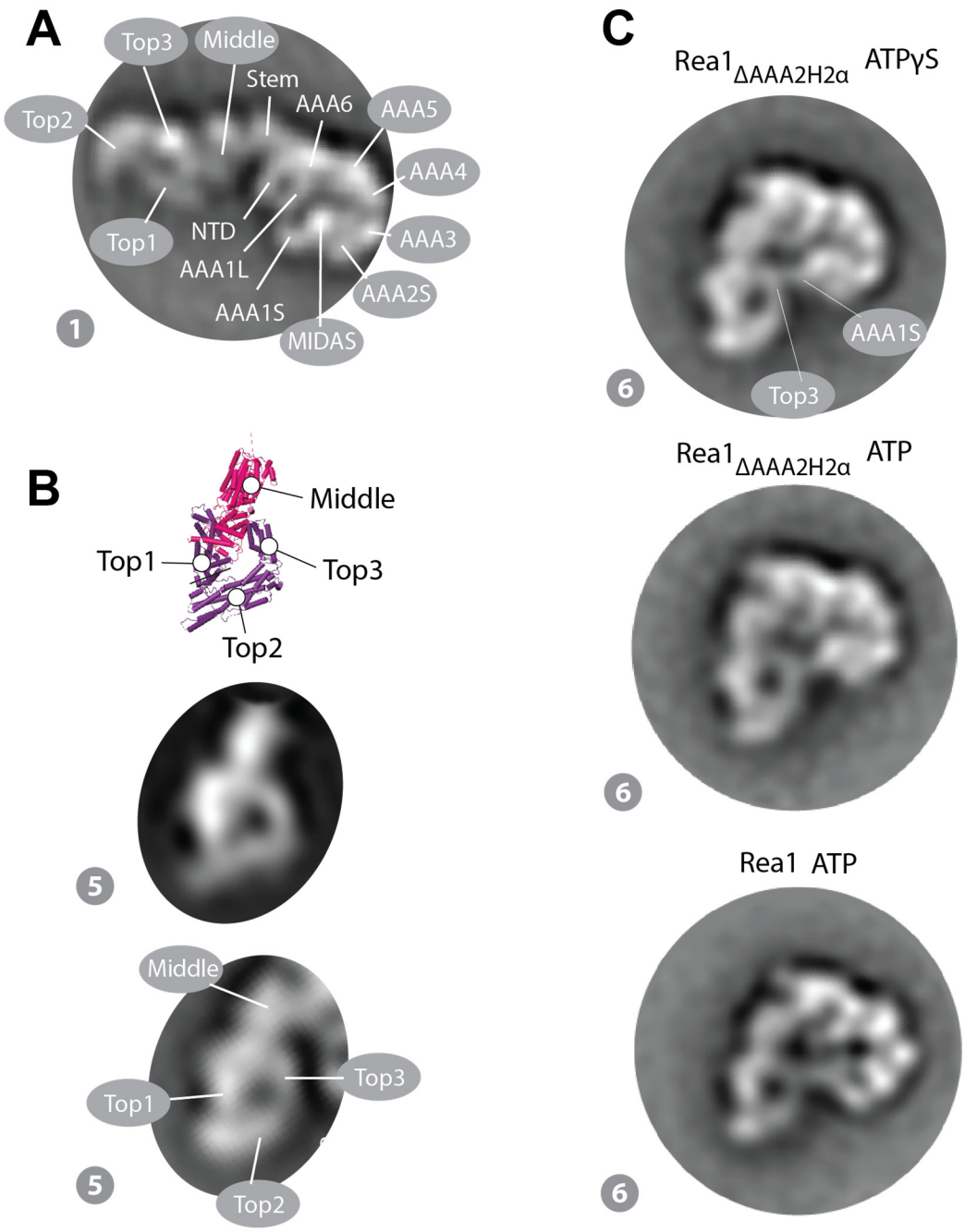

Supplementary figure 8: State 6 of the AAA+ ring engaged linker conformations features a connection between AAA1S and the linker top3 domain. A. Domain assignments in the AAA+ ring and linker. **B.** Two upper panels: Linker middle and top domains rotated into state 5 and corresponding cryoEM map projection (Two upper panels, compare also supplementary figure 7). Lower panel: Assignment of linker domains in state 5 based on the two upper panels. **C.** The domain assignments in A. and B. suggest a connection between AAA1S and the linker top3 domain in state 6. The connection is visible in three independently collected data sets.

Supplementary figure 9

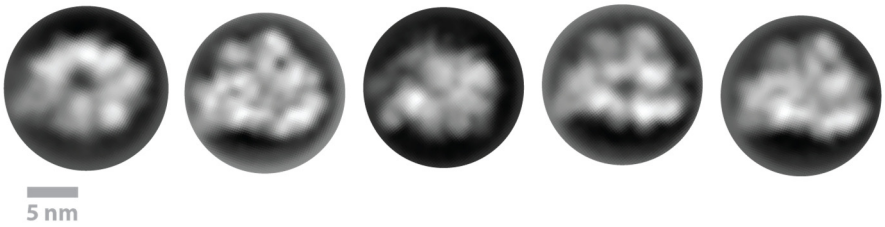

Supplementary figure 9: Negative stain 2D class averages of Rea1$_{\Delta 3072\text{-}3244}$ in the presence of ATP. There is no evidence for the linker indicating that the deletion of the globular extension of the middle domain (aa 3072-3244) leads to the degradation of the linker. The degradation of the linker is also supported by SDS-PAGE analysis. The size of the rings in the 2D class averages is comparable with the dimension of the Rea1 AAA+ ring (≈ 12 nm).

Supplementary figure 10

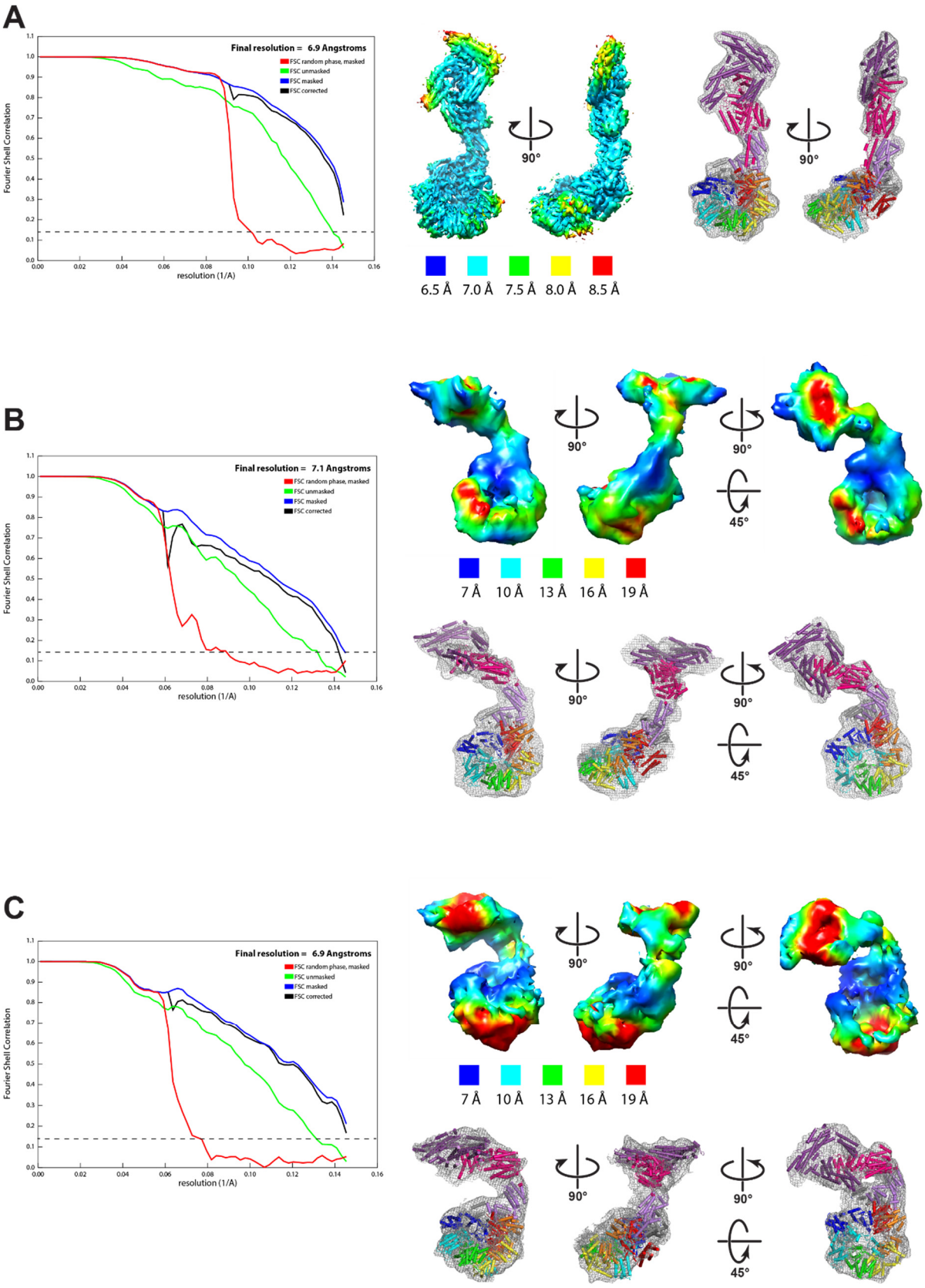

Supplementary figure 10: Overall quality of the Rea1$_{D2915A-R2976A-D3042A}$ ATP cryoEM maps. Fourier shell correlation (FSC) plot for half-maps of the 3D reconstructions (left panels, 0.143 FSC criteria is indicated as horizontal dashed line), local resolution maps (middle and right panels) and match of structure in map (right and lower right panels) of **A.** Conformation I, **B.** Conformation II and **C.** Conformation III. In

A. the resolution is of sufficient quality to identify secondary structure elements. In B. and C. the resolution is of sufficient quality to dock in the linker middle-top domains and the linker stem-AAA+ring-NTD as rigid bodies. Due to the use of binned data the 0.143 FSC criteria has not been reached in A. and C. No substantial improvements in the resolution are to be expected with the unbinned data.

Supplementary figure 11

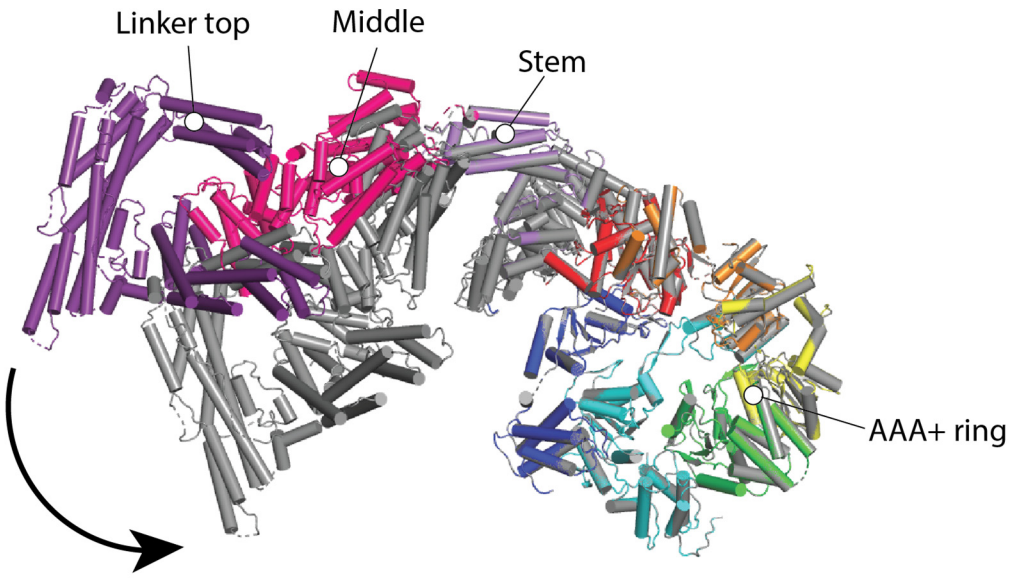

Supplementary figure 11: Conformations II and III of Rea1$_{D2915A-R2976A-D3042A}$ ATP are related by a swing of the linker middle and top domains towards the AAA+ ring. Conformation II is color coded, Conformation III is shown in grey. The structures have been aligned on the AAA+ rings. The black arrow indicates the swing towards the AAA+ ring.

Supplementary figure 12

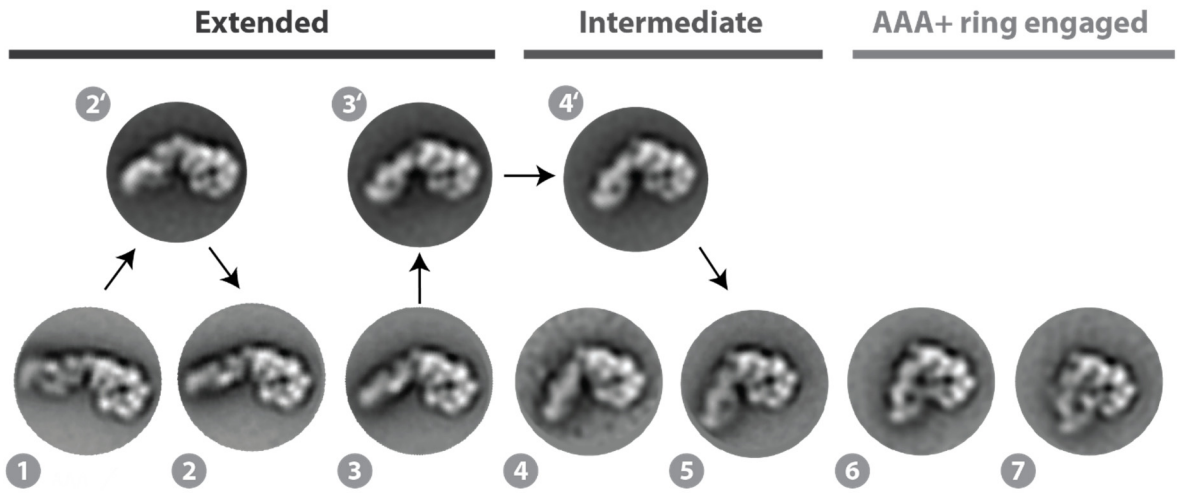

Supplementary figure 12: The swing and the rotation of the linker middle and top domains during linker remodelling are not strictly correlated. In addition to the linker states most commonly observed in our data sets (here states 1 – 7 of Rea1 wt ATP as an example), additional extended and intermediate linker remodelling states were occasionally detected. Linker state 2' represents a swing from state 1 towards the AAA+ ring without rotation. In state 3' the linker middle and top domains are already fully rotated before reaching the proximity of the AAA+ ring. They swing without rotation via state 4' to state 5.